The Astrophysical Journal Supplement Series, 240:23 (25pp), 2019 February https://doi.org/10.3847/1538-4365/aaf651

The Fifteenth Data Release of the Sloan Digital Sky Surveys: First Release of MaNGA-derived Quantities, Data Visualization Tools, and Stellar Library

D. S. Aguado[1], Romina Ahumada[2], Andrés Almeida[3], Scott F. Anderson[4], Brett H. Andrews[5], Borja Anguiano[6], Erik Aquino Ortíz[7], Alfonso Aragón-Salamanca[8], Maria Argudo-Fernández[9,10], Marie Aubert[11], Vladimir Avila-Reese[7], Carles Badenes[5], Sandro Barboza Rembold[12,13], Kat Barger[14], Jorge Barrera-Ballesteros[15], Dominic Bates[16], Julian Bautista[17], Rachael L. Beaton[18], Timothy C. Beers[19], Francesco Belfiore[20,21], Mariangela Bernardi[22], Matthew Bershady[23,24], Florian Beutler[17], Jonathan Bird[25], Dmitry Bizyaev[26,27], Guillermo A. Blanc[18], Michael R. Blanton[28], Michael Blomqvist[29], Adam S. Bolton[30], Médéric Boquien[9], Jura Borissova[31,32], Jo Bovy[33,34], William Nielsen Brandt[35,36,37], Jonathan Brinkmann[26], Joel R. Brownstein[38], Kevin Bundy[20], Adam Burgasser[39], Nell Byler[4], Mariana Cano Diaz[7,40], Michele Cappellari[41], Ricardo Carrera[42], Bernardo Cervantes Sodi[43], Yanping Chen[44], Brian Cherinka[45], Peter Doohyun Choi[46], Haeun Chung[47], Damien Coffey[48], Julia M. Comerford[49], Johan Comparat[48], Kevin Covey[50], Gabriele da Silva Ilha[12,13], Luiz da Costa[13,51], Yu Sophia Dai[52], Guillermo Damke[3,53], Jeremy Darling[49], Roger Davies[41], Kyle Dawson[38], Victoria de Sainte Agathe[54], Alice Deconto Machado[12,13], Agnese Del Moro[48], Nathan De Lee[25,55], Aleksandar M. Diamond-Stanic[56], Helena Domínguez Sánchez[22], John Donor[14], Niv Drory[57], Hélion du Mas des Bourboux[38], Chris Duckworth[16], Tom Dwelly[48], Garrett Ebelke[6], Eric Emsellem[21,58], Stephanie Escoffier[11], José G. Fernández-Trincado[2,59,60], Diane Feuillet[61], Johanna-Laina Fischer[22], Scott W. Fleming[45], Amelia Fraser-McKelvie[8], Gordon Freischlad[26], Peter M. Frinchaboy[14], Hai Fu[62], Lluís Galbany[5], Rafael Garcia-Dias[1,63], D. A. García-Hernández[1,63], Luis Alberto Garma Oehmichen[7], Marcio Antonio Geimba Maia[13,51], Héctor Gil-Marín[64,65], Kathleen Grabowski[26], Meng Gu[66], Hong Guo[67], Jaewon Ha[46], Emily Harrington[68,69], Sten Hasselquist[70], Christian R. Hayes[6], Fred Hearty[35], Hector Hernandez Toledo[7], Harry Hicks[71], David W. Hogg[28], Kelly Holley-Bockelmann[25], Jon A. Holtzman[70], Bau-Ching Hsieh[72], Jason A. S. Hunt[34], Ho Seong Hwang[47], Héctor J. Ibarra-Medel[7], Camilo Eduardo Jimenez Angel[1,63], Jennifer Johnson[73], Amy Jones[74], Henrik Jönsson[75], Karen Kinemuchi[26,70], Juna Kollmeier[18], Coleman Krawczyk[17], Kathryn Kreckel[61], Sandor Kruk[41], Ivan Lacerna[32,76], Ting-Wen Lan[77], Richard R. Lane[32,78], David R. Law[45], Young-Bae Lee[46], Cheng Li[79], Jianhui Lian[17], Lihwai Lin (林俐暉)[72], Yen-Ting Lin[72], Chris Lintott[41], Dan Long[26], Penélope Longa-Peña[9], J. Ted Mackereth[80], Axel de la Macorra[81], Steven R. Majewski[6], Olena Malanushenko[26], Arturo Manchado[1,63,82], Claudia Maraston[17], Vivek Mariappan[35], Mariarosa Marinelli[83], Rui Marques-Chaves[1,63], Thomas Masseron[1,63], Karen L. Masters (何凱論)[17,69,108], Richard M. McDermid[84], Nicolás Medina Peña[31], Sofia Meneses-Goytia[17], Andrea Merloni[48], Michael Merrifield[8], Szabolcs Meszaros[85,109], Dante Minniti[32,86,87], Rebecca Minsley[56], Demitri Muna[88], Adam D. Myers[89], Preethi Nair[74], Janaina Correa do Nascimento[12,13], Jeffrey A. Newman[5], Christian Nitschelm[9], Matthew D Olmstead[90], Audrey Oravetz[26], Daniel Oravetz[26], René A. Ortega Minakata[7], Zach Pace[23], Nelson Padilla[78], Pedro A. Palicio[1,63], Kaike Pan[26], Hsi-An Pan[72], Taniya Parikh[17], James Parker, III[26], Sebastien Peirani[91], Samantha Penny[17], Will J. Percival[17,92,93], Ismael Perez-Fournon[1,63], Thomas Peterken[8], Marc H. Pinsonneault[73], Abhishek Prakash[94], M. Jordan Raddick[15], Anand Raichoor[95], Rogemar A. Riffel[12,13], Rogério Riffel[13,96], Hans-Walter Rix[61], Annie C. Robin[60], Alexandre Roman-Lopes[97], Benjamin Rose[19], Ashley J. Ross[88], Graziano Rossi[46], Kate Rowlands[15], Kate H. R. Rubin[98], Sebastián F. Sánchez[7], José R. Sánchez-Gallego[4], Conor Sayres[4], Adam Schaefer[23], Ricardo P. Schiavon[80], Jaderson S. Schimoia[12,13], Edward Schlafly[99], David Schlegel[99], Donald P. Schneider[35,36], Mathias Schultheis[100], Hee-Jong Seo[101], Shoaib J. Shamsi[69], Zhengyi Shao[67], Shiyin Shen[67], Shravan Shetty[23], Gregory Simonian[73], Rebecca J. Smethurst[8,41], Jennifer Sobeck[4], Barbara J. Souter[15], Ashley Spindler[102], David V. Stark[77], Keivan G. Stassun[25], Matthias Steinmetz[103], Thaisa Storchi-Bergmann[13,96], Guy S. Stringfellow[49], Genaro Suárez[104], Jing Sun[14], Manuchehr Taghizadeh-Popp[15,105], Michael S. Talbot[38], Jamie Tayar[73], Aniruddha R. Thakar[15], Daniel Thomas[17], Patricia Tissera[86], Rita Tojeiro[16], Nicholas W. Troup[6], Eduardo Unda-Sanzana[9], Octavio Valenzuela[7], Mariana Vargas-Magaña[81], José Antonio Vázquez-Mata[7], David Wake[106], Benjamin Alan Weaver[30], Anne-Marie Weijmans[16], Kyle B. Westfall[20], Vivienne Wild[16], John Wilson[6], Emily Woods[56], Renbin Yan[107], Meng Yang[16], Olga Zamora[1,63], Gail Zasowski[38], Kai Zhang[99], Zheng Zheng[52], Zheng Zheng[38], Guangtun Zhu[15,110], Joel C. Zinn[73], and Hu Zou[52]

[1] Instituto de Astrofísica de Canarias, E-38205 La Laguna, Tenerife, Spain
[2] Departamento de Astronomia, Casilla 160-C, Universidad de Concepcion, Concepcion, Chile
[3] Instituto de Investigación Multidisciplinario en Ciencia y Tecnología, Universidad de La Serena, Benavente 980, La Serena, Chile
[4] Department of Astronomy, Box 351580, University of Washington, Seattle, WA 98195, USA
[5] PITT PACC, Department of Physics and Astronomy, University of Pittsburgh, Pittsburgh, PA 15260, USA
[6] Department of Astronomy, University of Virginia, 530 McCormick Road, Charlottesville, VA 22904-4325, USA
[7] Instituto de Astronomía, Universidad Nacional Autónoma de México, A.P. 70-264, 04510, México, D.F., México
[8] School of Physics & Astronomy, University of Nottingham, Nottingham, NG7 2RD, UK
[9] Centro de Astronomía (CITEVA), Universidad de Antofagasta, Avenida Angamos 601 Antofagasta, Chile
[10] Chinese Academy of Sciences South America Center for Astronomy, China-Chile Joint Center for Astronomy, Camino El Observatorio 1515, Las Condes, Santiago, Chile
[11] Aix Marseille Univ, CNRS/IN2P3, CPPM, Marseille, France

[12] Departamento de Física, CCNE, Universidade Federal de Santa Maria, 97105-900, Santa Maria, RS, Brazil
[13] Laboratório Interinstitucional de e-Astronomia, 77 Rua General José Cristino, Rio de Janeiro, 20921-400, Brazil
[14] Department of Physics and Astronomy, Texas Christian University, Fort Worth, TX 76129, USA
[15] Department of Physics and Astronomy, Johns Hopkins University, 3400 N. Charles Street, Baltimore, MD 21218, USA
[16] School of Physics and Astronomy, University of St Andrews, North Haugh, St Andrews, KY16 9SS, UK
[17] Institute of Cosmology & Gravitation, University of Portsmouth, Dennis Sciama Building, Portsmouth, PO1 3FX, UK
[18] The Observatories of the Carnegie Institution for Science, 813 Santa Barbara St., Pasadena, CA 91101, USA
[19] Department of Physics and JINA Center for the Evolution of the Elements, University of Notre Dame, Notre Dame, IN 46556, USA
[20] University of California Observatories, University of California, Santa Cruz, CA 95064, USA
[21] European Southern Observatory, Karl-Schwarzschild-Str. 2, D-85748 Garching, Germany
[22] Department of Physics and Astronomy, University of Pennsylvania, Philadelphia, PA 19104, USA
[23] Department of Astronomy, University of Wisconsin-Madison, 475 N. Charter St., Madison, WI 53726, USA
[24] South African Astronomical Observatory, P.O. Box 9, Observatory 7935, Cape Town, South Africa
[25] Department of Physics & Astronomy, Vanderbilt University, 6301 Stevenson Center Lane, Nashville, TN 37235, USA
[26] Apache Point Observatory, P.O. Box 59, Sunspot, NM 88349, USA
[27] Sternberg Astronomical Institute, Moscow State University, Universitetskij pr. 13, 119991 Moscow, Russia
[28] Center for Cosmology and Particle Physics, Department of Physics, New York University, 726 Broadway, Room 1005, New York, NY 10003, USA
[29] Aix Marseille Univ, CNRS, LAM, Laboratoire d'Astrophysique de Marseille, Marseille, France
[30] National Optical Astronomy Observatory, 950 North Cherry Avenue, Tucson, AZ 85719, USA
[31] Instituto de Física y Astronomía, Universidad de Valparaíso, Av. Gran Bretaña 1111, Playa Ancha, Casilla 5030, Chile
[32] Instituto Milenio de Astrofísica, Av. Vicuña Mackenna 4860, Macul, Santiago, Chile
[33] Department of Astronomy and Astrophysics, University of Toronto, 50 St. George Street, Toronto, ON, M5S 3H4, Canada
[34] Dunlap Institute for Astronomy and Astrophysics, University of Toronto, 50 St. George Street, Toronto, Ontario M5S 3H4, Canada
[35] Department of Astronomy and Astrophysics, Eberly College of Science, The Pennsylvania State University, 525 Davey Laboratory, University Park, PA 16802, USA
[36] Institute for Gravitation and the Cosmos, The Pennsylvania State University, University Park, PA 16802, USA
[37] Department of Physics, The Pennsylvania State University, University Park, PA 16802, USA
[38] Department of Physics and Astronomy, University of Utah, 115 S. 1400 E., Salt Lake City, UT 84112, USA
[39] Center for Astrophysics and Space Science, University of California San Diego, La Jolla, CA 92093, USA
[40] CONACYT Research Fellow - Instituto de Astronomía, Universidad Nacional Autónoma de México, A.P. 70-264, 04510, D.F., México
[41] Sub-department of Astrophysics, Department of Physics, University of Oxford, Denys Wilkinson Building, Keble Road, Oxford OX1 3RH, UK
[42] Astronomical Observatory of Padova, National Institute of Astrophysics, Vicolo Osservatorio 5, I-35122—Padova, Italy
[43] Instituto de Radioastronomía y Astrofísica, Universidad Nacional Autónoma de México, Campus Morelia, A.P. 3-72, C.P. 58089 Michoacán, México
[44] New York University Abu Dhabi, P.O. BOX 129188, Abu Dhabi, UAE
[45] Space Telescope Science Institute, 3700 San Martin Drive, Baltimore, MD 21218, USA
[46] Department of Astronomy and Space Science, Sejong University, Seoul 143-747, Republic of Korea
[47] Korea Institute for Advanced Study, 85 Hoegiro, Dongdaemun-gu, Seoul 02455, Republic of Korea
[48] Max-Planck-Institut für extraterrestrische Physik, Gießenbachstr. 1, D-85748 Garching, Germany
[49] Center for Astrophysics and Space Astronomy, Department of Astrophysical and Planetary Sciences, University of Colorado, 389 UCB, Boulder, CO 80309-0389, USA
[50] Department of Physics and Astronomy, Western Washington University, 516 High Street, Bellingham, WA 98225, USA
[51] Observatório Nacional, R. Gal. Jose Cristino 77, Rio de Janeiro, RJ 20921-400, Brazil
[52] National Astronomical Observatories, Chinese Academy of Sciences, 20A Datun Road, Chaoyang District, Beijing 100012, People's Republic of China
[53] AURA Observatory in Chile, Cisternas 1500, La Serena, Chile
[54] LPNHE, CNRS/IN2P3, Université Pierre et Marie Curie Paris 6, Université Denis Diderot Paris, 4 place Jussieu, F-75252 Paris CEDEX, France
[55] Department of Physics, Geology, and Engineering Technology, Northern Kentucky University, Highland Heights, KY 41099, USA
[56] Department of Physics and Astronomy, Bates College, 44 Campus Avenue, Lewiston, ME 04240, USA
[57] McDonald Observatory, The University of Texas at Austin, 1 University Station, Austin, TX 78712, USA
[58] Univ Lyon, Univ Lyon 1, Ens de Lyon, CNRS, Centre de Recherche Astrophysique de Lyon UMR5574, F-69230, Saint-Genis-Laval, France
[59] Instituto de Astronomía y Ciencias Planetarias, Universidad de Atacama, Copayapu 485, Copiapó, Chile
[60] Institut UTINAM, CNRS UMR6213, Univ. Bourgogne Franche-Comté, OSU THETA Franche-Comté-Bourgogne, Observatoire de Besançon, BP 1615, F-25010 Besançon Cedex, France
[61] Max-Planck-Institut für Astronomie, Königstuhl 17, D-69117 Heidelberg, Germany
[62] Department of Physics & Astronomy, University of Iowa, Iowa City, IA 52245, USA
[63] Departamento de Astrofísica, Universidad de La Laguna (ULL), E-38206 La Laguna, Tenerife, Spain
[64] Sorbonne Universités, Institut Lagrange de Paris (ILP), 98 bis Boulevard Arago, F-75014 Paris, France
[65] Laboratoire de Physique Nucléaire et de Hautes Energies, Université Pierre et Marie Curie, 4 Place Jussieu, F-75005 Paris, France
[66] Harvard-Smithsonian Center for Astrophysics, 60 Garden St., Cambridge, MA 02138, USA
[67] Shanghai Astronomical Observatory, Chinese Academy of Sciences, 80 Nandan Road, Shanghai 200030, People's Republic of China
[68] Department of Physics, Bryn Mawr College, Bryn Mawr, PA 19010, USA
[69] Department of Physics and Astronomy, Haverford College, 370 Lancaster Avenue, Haverford, PA 19041, USA; spokesperson@sdss.org
[70] Department of Astronomy, New Mexico State University, Box 30001, MSC 4500, Las Cruces, NM 88003, USA
[71] School of Maths and Physics, University of Portsmouth, Portsmouth, PO1 3FX, UK
[72] Academia Sinica Institute of Astronomy and Astrophysics, P.O. Box 23-141, Taipei 10617, Taiwan
[73] Department of Astronomy, Ohio State University, 140 W. 18th Ave., Columbus, OH 43210, USA
[74] Department of Physics and Astronomy, University of Alabama, Tuscaloosa, AL 35487-0324, USA
[75] Lund Observatory, Department of Astronomy and Theoretical Physics, Lund University, Box 43, SE-22100 Lund, Sweden
[76] Instituto de Astronomía, Universidad Católica del Norte, Av. Angamos 0610, Antofagasta, Chile
[77] Kavli Institute for the Physics and Mathematics of the Universe, Todai Institutes for Advanced Study, the University of Tokyo, Kashiwa, 277-8583, Japan
[78] Instituto de Astrofísica, Pontificia Universidad Católica de Chile, Av. Vicuna Mackenna 4860, 782-0436 Macul, Santiago, Chile
[79] Tsinghua Center for Astrophysics & Department of Physics, Tsinghua University, Beijing 100084, People's Republic of China
[80] Astrophysics Research Institute, Liverpool John Moores University, IC2, Liverpool Science Park, 146 Brownlow Hill, Liverpool L3 5RF, UK
[81] Instituto de Física, Universidad Nacional Autónoma de México, Apdo. Postal 20-364, México
[82] Consejo Superior de Investigaciones Científicas, Spain; amt@iac.es
[83] Department of Physics, Virginia Commonwealth University, Richmond, VA 23220-4116, USA
[84] Department of Physics and Astronomy, Macquarie University, Sydney NSW 2109, Australia

[85] ELTE Gothard Astrophysical Observatory, H-9704 Szombathely, Szent Imre herceg st. 112, Hungary
[86] Departamento de Física, Facultad de Ciencias Exactas, Universidad Andres Bello, Av. Fernandez Concha 700, Las Condes, Santiago, Chile
[87] Vatican Observatory, V00120 Vatican City State, Italy
[88] Center for Cosmology and AstroParticle Physics, The Ohio State University, 191 W. Woodruff Avenue, Columbus, OH 43210, USA
[89] Department of Physics and Astronomy, University of Wyoming, Laramie, WY 82071, USA
[90] Kings College, 133 North River Street, Wilkes-Barre, PA 18711, USA
[91] Institut d'Astropysique de Paris, UMR 7095, CNRS—UPMC, 98bis bd Arago, F-75014 Paris, France
[92] Department of Physics and Astronomy, University of Waterloo, 200 University Ave W, Waterloo, ON N2L 3G1, Canada
[93] Perimeter Institute for Theoretical Physics, 31 Caroline St. North, Waterloo, ON N2L 2Y5, Canada
[94] Infrared Processing and Analysis Center, California Institute of Technology, MC 100-22, 1200 E California Boulevard, Pasadena, CA 91125, USA
[95] Institute of Physics, Laboratory of Astrophysics, Ecole Polytechnique Fédérale de Lausanne (EPFL), Observatoire de Sauverny, 1290 Versoix, Switzerland
[96] Instituto de Física, Universidade Federal do Rio Grande do Sul Av. Bento Gonçalves 9500, CEP 91501-970, Porto Alegre, RS, Brazil
[97] Departamento de Física, Facultad de Ciencias, Universidad de La Serena, Cisternas 1200, La Serena, Chile
[98] Department of Astronomy, San Diego State University, San Diego, CA 92182, USA
[99] Lawrence Berkeley National Laboratory, 1 Cyclotron Road, Berkeley, CA 94720, USA
[100] Laboratoire Lagrange, Université Côte d'Azur, Observatoire de la Côte d'Azur, CNRS, Blvd de l'Observatoire, F-06304 Nice, France
[101] Department of Physics and Astronomy, Ohio University, Clippinger Labs, Athens, OH 45701, USA
[102] Department of Physical Sciences, The Open University, Milton Keynes, MK7 6AA, UK
[103] Leibniz-Institut für Astrophysik Potsdam (AIP), An der Sternwarte 16, D-14482 Potsdam, Germany
[104] Instituto de Astronomía, Universidad Nacional Autónoma de México, Unidad Académica en Ensenada, Ensenada BC 22860, México
[105] Institute for Data Intensive Engineering and Science, Johns Hopkins University, 3400 N. Charles Street, Baltimore, MD 21218, USA
[106] Department of Physics, University of North Carolina Asheville, One University Heights, Asheville, NC 28804, USA
[107] Department of Physics and Astronomy, University of Kentucky, 505 Rose Street, Lexington, KY, 40506-0055, USA
Received 2018 August 2; revised 2018 November 30; accepted 2018 December 3; published 2019 January 31

Abstract

Twenty years have passed since first light for the Sloan Digital Sky Survey (SDSS). Here, we release data taken by the fourth phase of SDSS (SDSS-IV) across its first three years of operation (2014 July–2017 July). This is the third data release for SDSS-IV, and the 15th from SDSS (Data Release Fifteen; DR15). New data come from MaNGA—we release 4824 data cubes, as well as the first stellar spectra in the MaNGA Stellar Library (MaStar), the first set of survey-supported analysis products (e.g., stellar and gas kinematics, emission-line and other maps) from the MaNGA Data Analysis Pipeline, and a new data visualization and access tool we call "Marvin." The next data release, DR16, will include new data from both APOGEE-2 and eBOSS; those surveys release no new data here, but we document updates and corrections to their data processing pipelines. The release is cumulative; it also includes the most recent reductions and calibrations of all data taken by SDSS since first light. In this paper, we describe the location and format of the data and tools and cite technical references describing how it was obtained and processed. The SDSS website (www.sdss.org) has also been updated, providing links to data downloads, tutorials, and examples of data use. Although SDSS-IV will continue to collect astronomical data until 2020, and will be followed by SDSS-V (2020–2025), we end this paper by describing plans to ensure the sustainability of the SDSS data archive for many years beyond the collection of data.

Key words: atlases – catalogs – surveys

1. Introduction

The Sloan Digital Sky Survey (SDSS; York et al. 2000) data releases began with the Early Data Release, or EDR, in 2001 June (Stoughton et al. 2002) and have been heavily used by astronomers and the broader public since that time (Raddick et al. 2014a, 2014b). Here, we present the 15th public data release from SDSS, or DR15, made publicly available on 2018 December 10.

SDSS has been marked by four phases so far, with plans for a fifth. Details are available in the papers describing SDSS-I (EDR, DR1–DR5; York et al. 2000), SDSS-II (DR6–DR7; Frieman et al. 2008; Yanny et al. 2009), SDSS-III (DR8–DR12; Eisenstein et al. 2011), and SDSS-IV (DR13–DR15; Blanton et al. 2017). Kollmeier et al. (2017) described the plans for SDSS-V, to start in mid-2020.

The data releases contain information about SDSS optical broadband imaging, optical spectroscopy, and infrared spectroscopy. Currently, SDSS-IV conducts optical and infrared spectroscopy (using two dedicated spectrographs; Smee et al. 2013; Wilson et al. 2018) at the 2.5 m Sloan Foundation Telescope at Apache Point Observatory (APO; Gunn et al. 2006) and infrared spectroscopy at the du Pont Telescope at Las Campanas Observatory (LCO; Bowen & Vaughan 1973).

SDSS-IV began observations in 2014 July and consists of three programs:

1. The extended Baryon Oscillation Spectroscopic Survey (eBOSS; Dawson et al. 2016) is surveying galaxies and quasars at redshifts $z \sim 0.6$–3.5 for large- scale structure. It includes two major subprograms:
   (a) The SPectroscopic IDentification of ERosita Sources (SPIDERS; Dwelly et al. 2017) investigates the nature of *X*-ray-emitting sources, including active galactic nuclei (AGNs) and galaxy clusters.

[108] SDSS-IV Spokesperson.
[109] Premium Postdoctoral Fellow of the Hungarian Academy of Sciences.
[110] Hubble Fellow.

   (b) The Time Domain Spectroscopic Survey (TDSS; Morganson et al. 2015) is exploring the physical nature of time-variable sources through spectroscopy.
2. Mapping Nearby Galaxies at APO (MaNGA; Bundy et al. 2015) uses integral-field spectroscopy (IFS) to study a representative sample of ∼10,000 nearby galaxies.
3. APOGEE-2 (the second phase of the APO Galactic Evolution Experiment or APOGEE; Majewski et al. 2017) performs a large-scale and systematic investigation of the entire Milky Way with near-infrared, high-resolution, and multiplexed instrumentation.

SDSS-IV has had two previous data releases (DR13 and DR14; Albareti et al. 2017 and Abolfathi et al. 2018, respectively), which contain the first two years of eBOSS, MaNGA, and APOGEE-2 data and new calibrations of the SDSS imaging data set.

DR15 contains new reductions and new data from MaNGA. This release includes the first three years of MaNGA data plus a new suite of derived data products based on the MaNGA data cubes, a new data access tool for MaNGA known as Marvin, and data from a large ancillary program aimed at improving the stellar library available for MaNGA (MaStar; the MaNGA Stellar Library).

The full scope of the data release is described in Section 2, and information on the data distribution is given in Section 3. Each of the subsurveys is described in its own section, with MaNGA in Section 4 and APOGEE-2 and eBOSS (including SPIDERS and TDSS) in Sections 5.1 and 5.2, respectively. We discuss future plans for SDSS-IV and beyond in Section 6. Readers wanting a glossary of terms and acronyms used in SDSS can find one at https://www.sdss.org/dr15/help/glossary/.

Table 1
Reduced SDSS-IV Spectroscopic Data in DR15

Target Category	# DR13	# DR13+14	# DR13 +14+15
eBOSS			
LRG samples	32,968	138,777	138,777
ELG Pilot Survey	14,459	35,094	35,094
Main QSO Sample	33,928	188,277	188,277
Variability Selected QSOs	22,756	87,270	87,270
Other QSO samples	24,840	43,502	43,502
TDSS Targets	17,927	57,675	57,675
SPIDERS Targets	3133	16,394	16,394
Standard Stars/White Dwarfs	53,584	63,880	63,880
APOGEE-2			
All Stars	16,4562	263,444	263,444
NMSU 1 m stars	894	1018	1018
Telluric stars	17,293	27,127	27,127
APOGEE-N Commissioning stars	11,917	12,194	12,194
MaNGA Cubes	1390	2812	4824
MaNGA main galaxy sample:			
PRIMARY_v1_2	600	1278	2126
SECONDARY_v1_2	473	947	1665
COLOR-ENHANCED_v1_2	216	447	710
MaStar (MaNGA Stellar Library)	0	0	3326
Other MaNGA ancillary targets[a]	31	121	324

Note.
[a] Many MaNGA ancillary targets were also observed as part of the main galaxy sample and are counted twice in this table; some ancillary targets are not galaxies.

2. Scope of Data Release 15

As with all previous SDSS public data releases, DR15 is cumulative and includes all data products that have been publicly released in earlier SDSS data releases. All previous releases are archived online to facilitate science replication; however, we recommend new users always make use of the latest DR (even when using older data) to ensure they are using the most recent reduction routines. The scope of DR15 is shown in Table 1, and its components can be summarized as follows.

1. MaNGA integral-field spectroscopic data from 285 plates, including 119 plates observed between 2016 September 26 (MJD 57658) and 2017 June 29 (MJD 57934) that are newly released data in DR15. This data set is identical to the internally released MaNGA Product Launch-7 (MPL-7) and contains the same set of galaxies but processed with a different version of the reduction pipeline from the earlier internally released MPL-6. DR15 contains 4824 reconstructed 3D data cubes, of which 4688 are target galaxies (the remainder are ancillary targets, which include galaxies, parts of galaxies, and some deep sky fields). This data set includes 67 repeat observations, so that the total number of unique galaxies in this data release is 4621. Most of these galaxies are part of the MaNGA main sample, but ancillary target galaxies are also included in this count (see Table 4 for a summary of these).
2. In addition to the MaNGA data cubes, DR15 also releases for the first time data products generated by the Data Analysis Pipeline (see Section 4.1.2). These products are available for all data cubes in DR15, with the exception of the cubes generated by some ancillary programs (i.e., Coma, IC 342, and M31) if they do not have redshifts (e.g., sky fields).
3. Alongside the new MaNGA data, and data products, DR15 also marks the launch of Marvin, a new tool to visualize and analyze MaNGA data cubes and maps (see Section 4.2).
4. DR15 is the first public data release for the MaNGA Stellar Library, MaStar (see Section 4.3), which contains 3326 optical stellar spectra.
5. In addition to updates to two previously released Value Added Catalogs (VACs), DR15 also includes six new VACs contributed by the MaNGA team (see Table 2). This brings the total number of VACs in the SDSS public data releases to 40.
6. Finally, DR15 includes a re-release of all previous versions of SDSS data releases. This includes the most recent data releases for APOGEE-2 and eBOSS (described in Abolfathi et al. 2018, DR14), and the most recent release of the SDSS imaging data (described in Albareti et al. 2017, DR13). Data of previous SDSS surveys are also included: the Legacy Spectra were finalized in DR8 (Aihara et al. 2011), and the SEGUE-1 and SEGUE-2 spectra in DR9 (Ahn et al. 2012). The

Table 2
New or Updated Value Added Catalogs

Description	Section	Reference(s)
Mini data release, 2018 Jul 31		
eBOSS DR14 QSO LSS catalogs	Section 5.2	Ata et al. (2018)
eBOSS DR14 LRG LSS catalogs	Section 5.2	Bautista et al. (2018)
Optical emission-line properties and black hole mass Estimates for SPIDERS DR14 Quasars	Section 5.3	Coffey et al. (2018)
Open Cluster Chemical Abundance and Mapping catalog DR15, 2018 Dec 10	Section 5.1.2	Donor et al. (2018)
GEMA-VAC: Galaxy Environment for MaNGA VAC	Section 4.5.4	M. Argudo-Fernandez et al. (2019, in preparation)
MaNGA Spectroscopic Redshifts	Section 4.5.5	Talbot et al. (2018)
MaNGA Pipe3D: Spatially resolved and integrated Properties of DR15 MaNGA galaxies[a]	Section 4.5.1	Sánchez et al. (2016, 2018)
MaNGA Firefly Stellar Populations[a]	Section 4.5.1	Goddard et al. (2017a), Wilkinson et al. (2017), Parikh et al. (2018)
MaNGA PyMorph DR15 photometric catalog	Section 4.5.2	Fischer et al. (2018)
MaNGA Morphology Deep Learning DR15 catalog	Section 4.5.2	Domínguez Sánchez et al. (2018)
H I-MaNGA Data Release 1	Section 4.5.3	Masters et al. (2018)
MaNGA Morphologies from Galaxy Zoo	Section 4.5.2	Willett et al. (2013), Hart et al. (2016)

Note.
[a] Update to DR14 VAC.

MARVELS spectra were last re-reduced for DR12 (Alam et al. 2015).

3. Data Distribution

The DR15 data can be accessed through a variety of mechanisms, depending on the type of data file and the needs of the user. All data access methods are described on the SDSS website (https://www.sdss.org/dr15/data_access), and we also provide tutorials and examples for accessing and working with SDSS data products at https://www.sdss.org/dr15/tutorials. We describe our four main data access mechanisms below.

All raw and processed imaging and spectroscopic data can be accessed through the Science Archive Server (SAS, https://data.sdss.org/sas/dr15). This site includes intermediate data products and VACs. The SAS is a file-based system, from which data can be directly downloaded by browsing or in bulk mode using rsync, wget, or Globus Online. Bulk downloading methods are outlined at https://www.sdss.org/dr15/data_access/bulk. All data files available on the SAS have a data model (https://data.sdss.org/datamodel), which provides a detailed overview of the content of each data file.

Processed optical and infrared spectra, as well as processed imaging, can also be accessed on the SAS through the Science Archive Webapp (SAW), an interactive web application (webapp; http://dr15.sdss.org links to the DR15 version). In DR15, the SAW is serving MaStar spectra for the first time. Through this webapp, users can display individual spectra and overlay model fits included on the SAS. There is a search option available to select spectra based on, e.g., plate number, coordinates, redshift, or ancillary observing program. Searches can be saved for future references as permalinks. Spectra can be directly downloaded from the SAS through the webapp, and links are included to the SkyServer Explore page for each object. The user can select SDSS data releases back to DR8 (the SAW was originally developed during SDSS-III so serves data from that phase of SDSS onwards only), but is encouraged to always use the most recent data release at https://data.sdss.org/home.

MaNGA data cubes and maps are not available in the SAW, but can be visualized and analyzed through Marvin. Marvin, described in detail in Section 4.2, provides links to the SAS for downloading data files, as well as the SkyServer Explore page.

The Catalog Archive Server (CAS; Thakar 2008; Thakar et al. 2008) stores the catalogs of DR15: these include photometric, spectroscopic, and derived properties. Some of the VACs also have catalogs that are stored on the CAS. The CAS can be accessed through the SkyServer webapp (https://skyserver.sdss.org), which provides Explore tools as well as the option of browser-based queries in synchronous mode. CASJobs (https://skyserver.sdss.org/casjobs) is suitable for more extensive queries, which are executed in asynchronous or batch mode, and offers users personal storage space for query results (Li & Thakar 2008). The CAS is integrated with SciServer (https://www.sciserver.org), which offers several data-driven science services, including SciServer Compute, a system that allows users to run Jupyter notebooks in Docker containers, directly accessing the SDSS catalogs.

All of the data reduction software that are used by the various SDSS-IV teams to reduce and process their data (including links to the Marvin Repository on Github) is publicly available at https://www.sdss.org/dr15/software/products.

4. MaNGA

The MaNGA survey uses a custom-built instrument (Drory et al. 2015), which feeds fibers from a suite of hexagonal bundles into the BOSS spectrograph (Smee et al. 2013). Over its planned five years of operations, MaNGA aims to get data for ~10,000 nearby galaxies (Law et al. 2015; Yan et al. 2016a, 2016b; see Wake et al. 2017 for details on the sample selection).

DR15 consists of MaNGA observations taken during the first three years of the survey (up to summer 2017) and nearly doubles the sample size of fully reduced galaxy data products previously released in DR14 (Abolfathi et al. 2018). These data products include raw data, intermediate reductions such as flux-calibrated spectra from individual exposures, and final data cubes and row-stacked spectra (RSS) produced using the

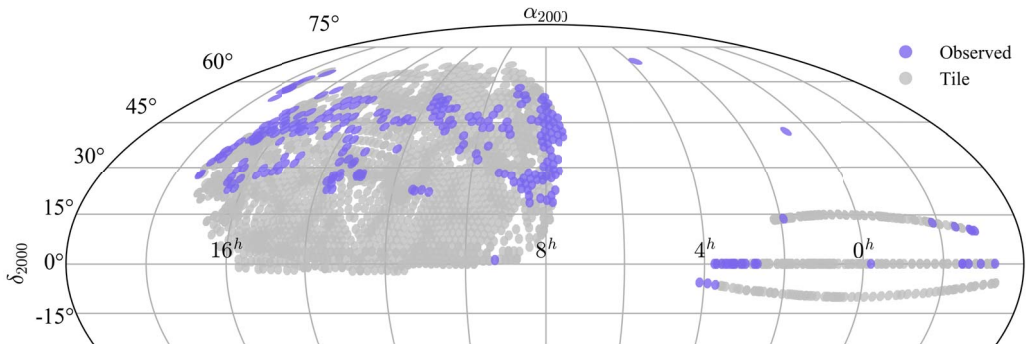

Figure 1. The sky distribution (Mollweide equatorial projection for decl. $>-20°$) of MaNGA plates released in DR15 (purple). This is overlaid on a plot of all possible MaNGA plates (in gray). MaNGA targets are selected from a sample with SDSS-I photometry and redshifts; hence, this footprint corresponds to Data Release 7 imaging data (Abazajian et al. 2009). Each plate contains 17 MaNGA targets, and around 30% of all possible plates will be observed in the full six-year survey. The most likely final footprint is indicated in Figure 2.

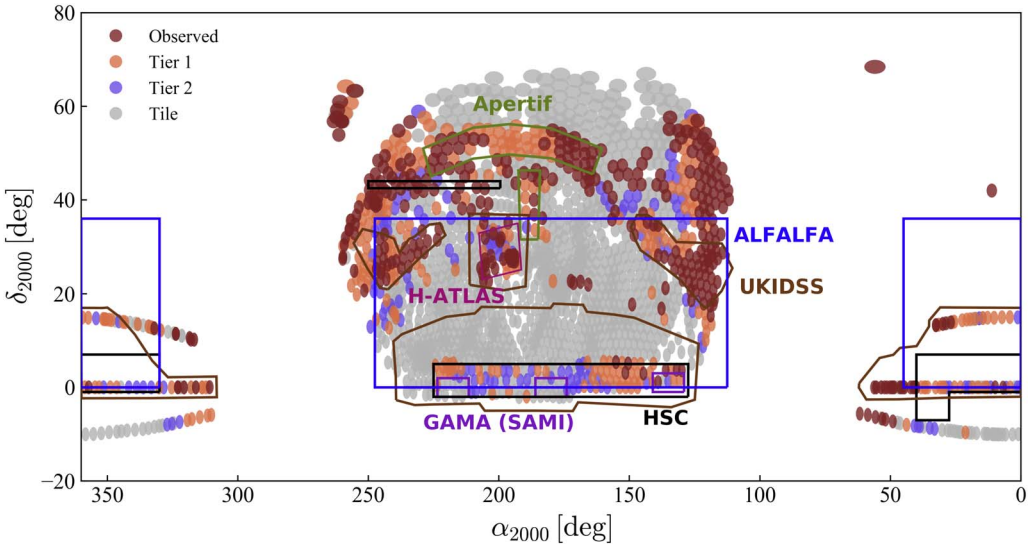

Figure 2. The sky distribution (in a rectangular projection for clarity) of the MaNGA projected final footprint overlaid with information about other surveys. Because MaNGA targets are selected from a sample with SDSS-I photometry and redshifts, the selection of all possible plates (gray) corresponds to Data Release 7 imaging data (Abazajian et al. 2009). Each plate contains 17 MaNGA targets, and around 30% of all possible plates will be observed in the full six-year survey; this plot indicates the likely final footprint for (a) typical weather conditions (Tier 1) and (b) good weather conditions (Tier 2). Completed plates noted on this plot show all observed plates at the time this was created, which is approximately one year of observing more than is being released in DR15. Where those plates are not filled in they have H I follow-up from the H I-MaNGA program (Masters et al. 2018; some, but not all of these data are released as a VAC in DR15—see Section 4.5.3). For the most up-to-date version of this plot, see https://www.sdss.org/surveys/manga/forecast/.

MaNGA Data Reduction Pipeline (DRP; Law et al. 2016). DR15 includes DRP data products for 4824 MaNGA cubes distributed among 285 plates, corresponding to 4621 unique galaxies plus 67 repeat observations and 118 special targets from the ancillary programs (see Section 4.4). Unlike in previous data releases, data cubes and summary RSS files are no longer produced for the 12 seven-fiber mini bundles on each plate that target bright stars and are used to derive the spectrophotometric calibration vector for each exposure (see Yan et al. 2016b); these observations will from here on instead be included in the MaStar stellar spectral library (see Section 4.3).

In addition, for the first time, DR15 includes the release of derived spectroscopic products (e.g., stellar kinematics, emission-line diagnostic maps, etc.) from the MaNGA DAP (Belfiore et al. 2019; Westfall et al. 2019); see Section 4.1.2.

We provide the sky footprint of MaNGA galaxies released in DR15 in Figure 1, while the projected final survey footprint is shown overlaid on the footprint of other relevant surveys and for two different expectations for weather at the telescope in Figure 2.

4.1. MaNGA Data and Data Products

4.1.1. The Data Reduction Pipeline

The MaNGA DRP is the IDL-based software suite that produces final flux-calibrated data cubes from the raw dispersed fiber spectra obtained at APO. The DRP is described in detail by Law et al. (2016) and consists of two stages. The "2d" DRP processes individual exposures, applying bias and overscan corrections, extracting the one-dimensional fiber spectra, sky-subtracting and flux-calibrating the spectra, and combining information from the four individual cameras in the BOSS spectrographs into a single set of RSS (`mgCFrame` files) on a common wavelength grid. The "3d" DRP uses astrometric information to combine the `mgCFrame` fiber spectra from individual exposures into a composite data cube on a regularized $0\farcs5$ grid, along with information about the inverse

variance, spaxel mask, instrumental resolution, and other key parameters. The `mgCFrame` per-exposure files are produced on both linear and logarithmic wavelength grids directly from the raw detector pixel sampling, and used to construct the corresponding logarithmic and linearly sampled data cubes.

The DRP data products released in DR15 are largely similar to those released in DR13 and DR14 (and identical to the internal collaboration release MPL-7) and consist of multi-extension FITS files giving the flux, inverse variance, mask, and other information for each object. The metadata from all of our observations are summarized in a FITS binary table, "`drpall-v2_4_3.fits`," detailing the coordinates, targeting information, redshift, data quality, etc. The version of the MaNGA DRP used for DR15 (`v2_4_3`)[111] incorporates some significant changes compared to the DR14 version of the pipeline (`v2_1_2`). These changes include the following:

1. The MaNGA DRP has been extended to produced one-dimensional reduced spectra for each of the MaStar targets observed during bright time; details of these modifications are described in Section 4.3.
2. DR15 introduces some significant changes in the overall flux calibration relative to DR13/DR14 (and relative to the description by Yan et al. 2016b). Foremost among these is the use of BOSZ stellar spectral models (Bohlin et al. 2017) instead of the original Kurucz templates built in 2003 to derive the spectrophotometric calibration based on contemporaneous observations of standard stars with the MaNGA seven-fiber mini bundles. Since the BOSZ templates picked by the pipeline are bluer by 0.03 mag in SDSS $u - r$ color than the version of the Kurucz models produced in 2003, this change slightly increases the overall flux blueward of 4000 Å in the MaNGA data cubes. Test observations of hot white dwarfs compared to ideal blackbody models generally show better performance using the new BOSZ calibration (as illustrated in Figure 3). Additionally, the throughput loss vector applied to the observational data is now smoother at many wavelengths; high-frequency basis spline fits are still used in telluric regions, but the spline has a much lower frequency outside the telluric regions to avoid introducing artifacts due to slight template mismatches. This significantly reduces the amount of artificially high-frequency, low-level (∼few percent) variations seen in the resulting spectra from earlier versions. The list of telluric regions is also updated.
3. Many aspects of the spectral line-spread function (LSF) estimation in the DRP have changed in DR15 in order to improve the level of agreement with independent estimates (observations of bright stars and galaxies previously observed at higher spectral resolution, observations of the solar spectrum, etc.). These changes include the use of a Gaussian comb method to propagate LSF estimates through the wavelength rectification step, computation of both pre-pixelized and post-pixelized LSF estimates,[112] improved interpolation over masked regions, and a modified arc lamp reference line list to improve LSF estimation and wavelength calibration in the far blue by rejecting poor-quality lines. The DRP data products contain additional extensions to describe this new information, including a 3D cube describing the effective LSF at each spaxel within the MaNGA data cube as a function of wavelength; this combines the information known about the LSF in each individual fiber spectrum to describe the net effect of stacking spectra with slightly different resolutions. The LSF changes and assessment against various observational calibrators will be described in greater detail by D. Law et al. (2019, in preparation).
4. The DRP data cubes now contain extensions describing the spatial covariance introduced in the data cubes by the cube-building algorithm. This information is provided in the form of sparse correlation matrices at the characteristic wavelengths of the SDSS *griz* filters and can be interpolated to estimate the correlation matrix at any other wavelength in the MaNGA data cubes. Note that the DR14 paper incorrectly stated that those data included these extensions. They did not (the team-internal MPL-5, which is the most similar MPL to DR14, did, but DR14 itself did not), so this is the first release of these extensions.
5. The `DRPall` summary file for DR15 contains 10 additional columns with respect to DR14. These columns include an estimate of the targeting redshift z that is used as the starting guess by the DAP when analyzing the MaNGA data cubes. z is generally identical to the NASA-Sloan Atlas (NSA) (Blanton et al. 2011) catalog redshift for the majority of MaNGA galaxies, but the origin of the redshift can vary for galaxies in the ∼25 MaNGA

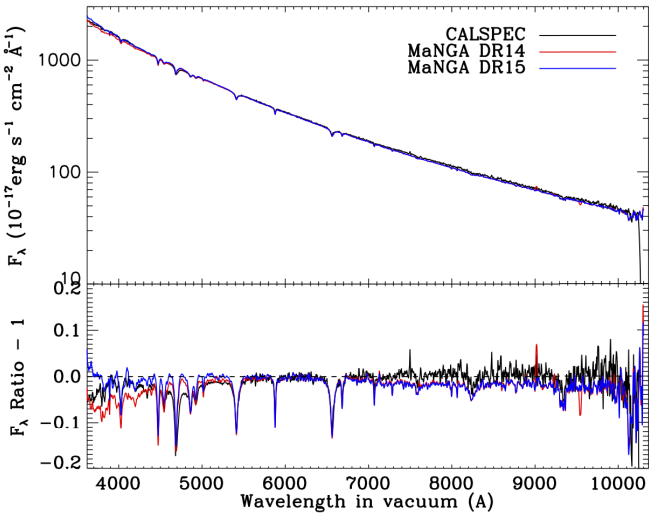

Figure 3. Flux calibration difference between DR14 and DR15 MaNGA data reductions. The upper panel shows the spectra for an Oke standard, HZ 21, a $T = 100{,}000$ K star (Oke & Shipman 1971; Reynolds et al. 2003), as given by the CALSPEC database (black) and by MaNGA in DR14 (red) and DR15 (blue) averaging over nine exposures taken on plate 7444. The small difference at the blue wavelengths can be seen more obviously in the bottom panel where we divide these three spectra by a $T = 100{,}000$ K blackbody spectrum normalized at 6000–6100 Å. Ignoring the absorption lines, this provides a test of our flux calibration. Using the BOSZ templates in DR15, the resulting continuum of this white dwarf agrees much better with the blackbody spectrum below 5000 Å, which is significantly improved compared to DR14, which uses the version of the Kurucz models (Kurucz 1979; Kurucz & Avrett 1981) produced in 2003, and to CALSPEC. (One can also compare this with Figure 9 of Yan et al. 2016b).

[111] https://svn.sdss.org/public/repo/manga/mangadrp/tags/v2_4_3

[112] That is, whether the best-fit Gaussian model of the lines is determined by evaluation at the pixel midpoints (post-pixelized) or integrated over the pixel boundaries (pre-pixelized). The two techniques can differ at the 10% level for marginally undersampled lines, and the appropriate value to use in later analyses depends on the fitting algorithm.

ancillary programs. Additional columns include a variety of estimates of the volume weights for the MaNGA primary and secondary galaxy samples.

6. Additional under-the-hood modifications to the DRP have been made for DR15 that provide minor bug fixes and performance improvements. These include modifications to the reference pixel flat fields for certain MJDs, updates to the reference bias and bad pixel masks, better rejection of saturated pixels, updates to the algorithms governing weighting of the wavelength rectification algorithm near ultrabright emission lines, etc. A detailed change log can be found in the DRP online repository.[113]

When working with the MaNGA data, note that there are several quality-control features that should be used to ensure the best scientific quality output. First, each MaNGA data cube has a FITS header keyword DRP3QUAL that describes the overall quality of the cube (identifying issues such as focus problems, flux-calibration problems, large numbers of dead fibers, etc.). About 1% of the data cubes are flagged as significantly problematic (i.e., have the CRITICAL quality bit set) and should be treated with extreme caution. Additionally, there is a 3d mask extension to each data cube that contains spaxel-by-spaxel information about problematic regions within the cube. This mask identifies issues such as dead fibers (which can cause local glitches and holes within the cube), foreground stars that should be masked by analysis packages such as the DAP, etc. Although the vast majority of cosmic rays and other transient features are detected by the DRP and flagged (either for removal or masking), lower intensity glitches (e.g., where the edge of a cosmic-ray track intersects with a bright emission line) can sometimes be missed and propagate into the final data cubes where they show up as unmasked hot pixels. Future improvements to the DRP may further address this issue, but caution is thus always advised when searching for isolated emission features in the data cubes.

For information on downloading MaNGA data in DR15, please see Section 3; new for DR15 is the Marvin interface to MaNGA data (see Section 4.2 below).

4.1.2. The Data Analysis Pipeline

The MaNGA DAP is the SDSS-IV software package that analyzes the data produced by the MaNGA DRP. The DAP currently focuses on "model-independent" properties, i.e., those relatively basic spectral properties that require minimal assumptions to derive. For DR15, these products include stellar and ionized-gas kinematics, nebular emission-line fluxes and equivalent widths, and spectral indices for numerous absorption features, such as the Lick indices (Worthey & Ottaviani 1997; Trager et al. 1998) and D4000 (Bruzual 1983). Examples of the DAP-provided measurements and model fits are shown in Figure 4, discussed through the rest of this section.

An overview of the DAP is provided by Westfall et al. (2019). There, we describe the general workflow of the pipeline, explain the detailed algorithm used for each of its primary products, provide high-level assessments of its performance, and describe the delivered data products in detail. In-depth assessments of the stellar kinematics, ionized-gas kinematics, emission-line fluxes, and emission-line equivalent widths are provided by Westfall et al. (2019) and Belfiore et al. (2019). All survey-provided properties are currently derived from the data cubes sampled in constant steps of the logarithm of the wavelength (i.e., the LOGCUBE files). However, the core functions are developed to consider each spectrum largely independently.

The DAP allows for a number of different options when analyzing the data, which we refer to as the analysis mode or DAPTYPE. In DR15, the DAPTYPE joins the keywords identifying the type of spatial binning applied (e.g., Voronoi-binned to signal-to-noise ratio (S/N) $\gtrsim$ 10, VOR10), the parametric form of the line-of-sight velocity distribution (LOSVD) used for the stellar kinematics (a Gaussian function, GAU), and the template set used to model the stellar continuum (a hierarchically clustered distillation of the MILES stellar library, MILESHC). For DR15, two DAPTYPEs have been made available, VOR10-GAU-MILESHC and HYB10-GAU-MILESHC. That is, only the binning approach differs between the two available DAPTYPEs, primarily distinguishing whether or not the main analysis steps are performed on binned spectra or individual spaxels. The stellar LOSVD is always assumed to be Gaussian, and the 42 templates resulting from a hierarchical clustering analysis of the MILES stellar library (Sánchez-Blázquez et al. 2006; Falcón-Barroso et al. 2011) are always used for the continuum templates; details regarding the latter are discussed in Westfall et al. (2019).

In the first mode (VOR10-GAU-MILESHC), the spaxels are binned using the Voronoi-binning scheme from Cappellari & Copin (2003) to a minimum g-band S/N of 10 per spectral pixel. The first mode then performs all subsequent analysis on those binned spectra. Alternatively, the second mode (HYB10-GAU-MILESHC) only performs the stellar kinematics on the binned spectra; the subsequent emission-line and spectral-index measurements are all performed on individual spaxels. This "hybrid" binning approach is likely the approach that most users will want to use in their analysis. The main exception to this is if any subsequent analyses depend on, e.g., the availability of emission-line models for the binned spectra, as is the case for the FIREFLY VAC (Wilkinson et al. 2017; see Section 4.5.1). The example data shown in Figure 4 are for observation 8138-12704 following from the hybrid-binning approach. Close inspection of the stellar velocity field will show that outermost regions have been binned together, all showing the same stellar velocity measurement. However, the Hα flux and D4000 maps have measurements for each spaxel.

The DAP is executed for all observations obtained by the MaNGA survey; however, some observations, primarily those obtained for our ancillary science programs, do not have all the required parameters currently needed as input by the DAP. Additionally, a few observations (<0.3%) trip corner failure modes of the DAP leading to errors in the construction of its main output files. These issues mean that not all LOGCUBE files provided by the DRP have associated DAP products. For those observations that are successfully analyzed (4718 in total), the DAP provides two main output files for each DAPTYPE, the MAPS file and the model LOGCUBE file. Examples of how to access and plot the data in these files are provided in a set of tutorials on the data-release website at https://www.sdss.org/dr15/manga/manga-tutorials/dap-tutorial/.

The MAPS file contains all of the derived properties organized as a series of maps, or images, that have the same on-sky projection as a single wavelength channel in the

[113] https://svn.sdss.org/public/repo/manga/mangadrp/tags/v2_4_3/RELEASE_NOTES

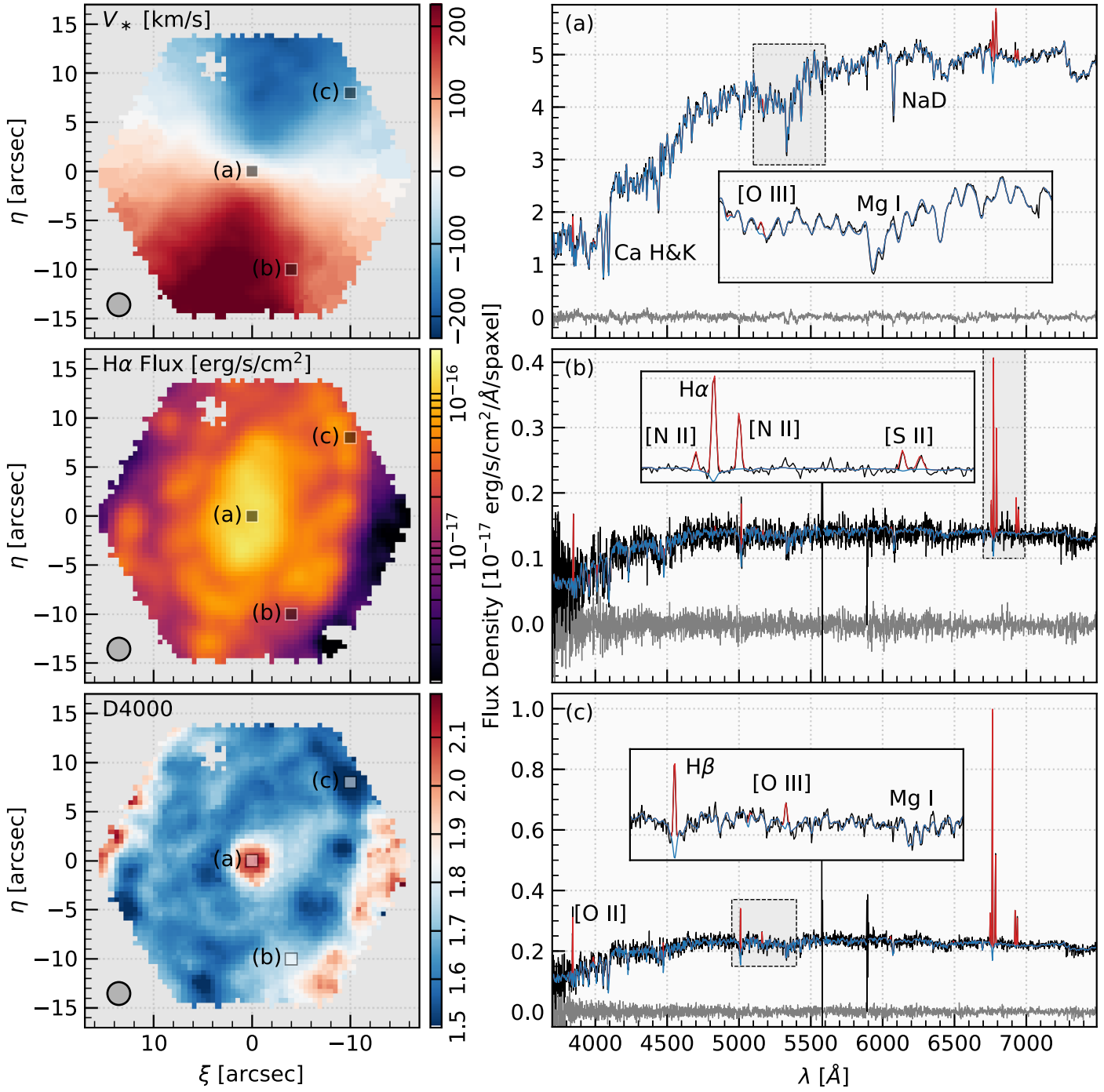

Figure 4. Example data provided by the MaNGA data analysis pipeline (DAP) for MaNGA observation 8138-12704, MaNGA ID 1-339041, following the hybrid-binning approach (`DAPTYPE` is `HYB10-GAU-MILESHC`). The left columns shows maps, or images, of some of the DAP-derived quantities, namely, from top to bottom, the stellar velocity field, Hα flux, and D4000 spectral index, where the measured value is indicated by the colorbar to the right of each map panel. The effective beam size for the MaNGA observations (FWHM $\sim 2\farcs5$) is shown by the gray circle in the bottom left of each map panel. Three spaxels are highlighted and labeled (a), (b), and (c), according to their spectra plotted in the right column. Each spectrum panel shows the observed MaNGA spectrum (black), stellar-continuum-only model (blue), and best-fitting (stars+emission lines) model (red); the residuals between the data (black) and the model (red) are shown in gray. Note that the red and blue lines are identical except for regions with nebular emission. A few salient emission and absorption features are marked in each panel. Inset panels provide a more detailed view of the quality of the fitted models in the regions highlighted by gray boxes. The spectrum panels only show the spectral regions fit by the DAP, which is limited by the MILES spectral range for DR15.

analyzed DRP `LOGCUBE` file. The images in the left panels of Figure 4 are example maps taken from the DAP `MAPS` file for observation 8138-12704. The maps are organized in a series of extensions grouped by the measurement they provide. Some extensions contain a single image with all of the relevant data, whereas other extensions have multiple images, one for, e.g., each of the measured emission lines. For example, the `STELLAR_VEL` extension has a single image with the measured single-component stellar velocity measured for each spatial bin (like that shown in Figure 4), while the `SPECINDEX` extension has 46 images, organized similarly to the wavelength channels in the DRP data cubes (the D4000

map shown in Figure 4 is in the 44th channel of the SPECINDEX extension).

The DAP-output model LOGCUBE file provides both the S/N-binned spectra and the best-fitting model spectra. From these files, users can plot the best-fitting model spectra against the data, as demonstrated in Figure 4, as an assessment of the success of the DAP. This is particularly useful when a result of the fit, e.g., the Hα flux, seems questionable. Indeed, Westfall et al. (2019) note regimes where the DAP has not been appropriately tailored to provide a successful fit; this is particularly true for spectra with very broad emission lines, such as the broad-line regions of AGNs. Users are encouraged to make sure they are well aware of these limitations in the context of their science goals. Finally, in combination with the DRP LOGCUBE file, users can use the model LOGCUBE data to construct emission-line-only or stellar-continuum-only data cubes by subtracting the relevant model data.

Although we have endeavored to make the output data user-friendly, there are a few usage quirks of which users should be aware:

1. As with all SDSS data products, users are strongly encouraged to understand and use the provided quality flags, for those data provided as masks. The mask bits provide important information as to whether or not users should trust the provided measurements in their particular use case. The conservative approach of ignoring any measurement where the mask bit is nonzero is safe, at least in the sense of not including any measurements we know to be dubious. However, the DAP makes use of an UNRELIABLE flag that is intended to be more of a warning that users should consider how the measurements affect their science as opposed to an outright rejection of the value. The UNRELIABLE flag is put to limited use in DR15, only flagging measurements that hinge on bandpass integrals (emission-line moments and non-parametric equivalent widths, and spectral indices) where any pixels are masked within the bandpass. However, this bit may become more extensively used in future releases as we continue to vet the results of the analysis. A more extensive discussion of the mask bits and their usage is provided by Westfall et al. (2019).
2. To keep the format of the output files consistent with the DRP LOGCUBE files, the binned-spectra and binned-spectra measurements are repeated for each spaxel within a given bin. This means that, e.g., the stellar velocity dispersion measured for a given binned spectrum is provided in the output DAP map at the location of each spaxel in that bin. Of course, when analyzing the output, one should most often only be concerned with the unique measurements for each observation. To this end, we provide an extension in the MAPS file that provides a "bin ID" for each spaxel. Spaxels excluded from any analysis (as in the buffer region during the data cube construction) are given a bin ID of -1. This allows the user to select all of the unique measurements by finding the locations of all unique bin ID values, ignoring anything with a bin ID of -1. Tutorials for selecting the unique measurements in the DAP-output maps are provided via the data-release website at https://www.sdss.org/dr15/manga/manga-tutorials/dap-tutorial/.
3. Corrections that have not been applied to the data in the output files are provided for a few quantities in the MAPS file. The stellar velocity dispersion and ionized-gas velocity dispersions are provided as measured from the core pPXF software (Cappellari & Emsellem 2004; Cappellari 2017) used by the DAP. This means that any instrumental effects present during the fitting process are also present in the output data. For both the stellar and ionized-gas dispersions, we have estimated the instrumental corrections for each measurement and provided the result in extensions in the MAPS file. These corrections should be applied when using the data for science. For the velocity dispersion measurements, our purpose in not applying the corrections ourselves is to allow the user freedom in how they deal with measurements of the dispersion that are below our measurement of the instrumental resolution. Such issues can be pernicious at low velocity dispersion, and the treatment of these data can have significant effects on, e.g., the construction of a radially averaged velocity dispersion profile (see Westfall et al. 2019, who discuss this at length, and also Penny et al. 2016, who discuss this issue for dwarf galaxies). Corrections are also provided (but not applied) for the spectral indices to convert the measurement to zero velocity dispersion at the spectral resolution of the MILES stellar templates (Beifiori et al. 2011) used during the stellar-continuum fit. Additional details regarding these corrections are provided in Westfall et al. (2019), and tutorials demonstrating how to apply them to the data are provided via the data-release website.
4. In the hybrid-binning scheme, the stellar kinematics are performed on the binned spectra, but the emission-line fits are performed on the individual spaxels. When comparing the model to the data, the user must compare the emission-line modeling results to the DRP LOGCUBE spectra, not to the binned spectra provided in the DAP model LOGCUBE file, unless the "binned" spectrum is actually from a single spaxel. Tutorials for how to overplot the correct stellar-continuum and emission-line models are provided via the data-release website.

Finally, similar to the DRPall file provided by the MaNGA DRP, the DAP constructs a summary table called the DAPall file. This summary file collates useful data from the output DAP files, as well as providing some global quantities drawn from basic assessments of the output maps, that may be useful for sample selection. For example, the DAPall file provides the luminosity-weighted stellar velocity dispersion and integrated star formation rate within 1 R_e. The sophistication of these measurements is limited in some cases. For example, the star formation rate provided is simply based on the measured Hα luminosity and does not account for internal attenuation or sources of Hα emission that are unrelated to star formation; as such, we caution users to make use of this for science only after understanding the implications of this caveat. Development and refinement of DAPall output will continue based on internal and community input. Additional discussion of how these properties are derived is provided by Westfall et al. (2019).

4.2. Marvin Access to MaNGA

Marvin (Cherinka et al. 2018)[114] is a new tool designed for streamlined access to the MaNGA data, optimized for overcoming the challenges of searching, accessing, and visualizing the complexity of the MaNGA data set. Whereas previous generations of SDSS took spectra only of the centers of galaxies, MaNGA takes many spectra of each galaxy, in a hexagonal grid across the face of each (IFU bundle), which are combined into a final data cube. This means that for each object there is not a single spectrum, but in fact a suite of complex results in one or more data cubes. The motivation for Marvin arises from the additional complexity of MaNGA data, namely the spatial interconnectivity of its spectra.

Marvin allows the user to:

1. access reduced MaNGA data cubes locally, remotely, or via a web interface.
2. access and visualize data analysis products.
3. perform powerful queries on the metadata.
4. abstract the MaNGA data model and write code that is agnostic to where the data actually live.
5. make better visualization and scientific decisions by mitigating common mistakes when accessing these types of data.

Marvin has two main components: a webapp and a Python package of tools, both using an underlying Marvin API (or Application Programming Interface). The webapp, Marvin Web,[115] provides an easily accessible interface for searching the MaNGA data set and visual exploration of individual MaNGA galaxies. The Marvin suite of Python tools, Marvin Tools, provides seamless programmatic access to the MaNGA data for more in-depth scientific analysis and inclusion in your science workflow. Marvin contains a multimodal data access system that provides remote access to MaNGA files or subdata contained within, downloads MaNGA files to work with on the user's local machine, and seamlessly transitions between the two with a negligible change in syntax.

Existing 3d data cube visualizers in astronomy, as well as in other scientific disciplines, often come as standalone desktop applications designed to visualize and interact with individual files local to a client machine. However, these tools are highly specific, limited to exploring files one at a time, and still require manually downloading all data locally. Although Marvin is a tool for 3d cube visualization, its focus is on streamlined data access from local or remote sources, with a clear separation of components into browser-based visualization and programmatic data tools, rather than on providing yet another desktop-based cube viewer. Marvin's design allows for users to rapidly explore and access the data in a manner of their choosing, while still providing enough flexibility to, if desired, plug the data into existing cube viewers available in the astronomy community.

The components of Marvin are described in more detail in the Marvin paper (Cherinka et al. 2019) as well as in the Marvin documentation,[116] which also contains tutorials and example Jupyter notebooks. In addition, we briefly introduce them below.

4.2.1. Marvin Web

Marvin Web provides quick visual access to the set of MaNGA galaxies. It provides a dynamic, interactive, point-and-click view of individual galaxies to explore the output from the MaNGA DRP and DAP (Sections 4.1.1 and 4.1.2, respectively), along with galaxy information from the NSA catalog (Blanton et al. 2011).[117]

We show a screenshot of the View-Spectra page of Marvin Web in Figure 5. By clicking anywhere within the galaxy IFU bundle on the SDSS three-color image, or any Data Analysis 2D Map, the user can explore the spectrum at that location for quick inspection. The visualized spectrum is interactive as well, allowing panning and zooming.

Additional pages that Marvin Web provides are:

1. a Query page, for searching the MaNGA data set through an SQL-like interface;
2. a Plate page, containing all MaNGA galaxies observed on a given SDSS plate;
3. and an Image Roulette page, for randomly sampling images of MaNGA galaxies.

Tutorials for navigating Marvin Web can be found at https://www.sdss.org/dr15/manga/manga-tutorials/marvin-tutorial/marvin-web/.

Marvin Web is designed as a gateway to entry into real MaNGA data, providing commonly desired functionalities all in one location, as well as code snippets to help transition users into a more programmatic environment using the Marvin Tools.

4.2.2. The Marvin Tools

Marvin Tools provide a programmatic interaction with the MaNGA data, enabling rigorous and repeatable science-grade analyses. Marvin Tools come in the form of a Python package that provides convenience classes and functions that simplify the processes of searching, accessing, downloading, and interacting with MaNGA data; selecting a sample; running a user-defined analysis code; and producing publication-quality figures.

Marvin Tools are a pip-installable product, packaged under sdss-marvin, with full installation instructions at the Marvin documentation website[118] and the source code on Github.[119]

Overall, Marvin Tools allow for easier access to the data without knowing much about the data model, by seamlessly connecting all of the MaNGA data products, eliminating the need to micromanage a multitude of files. The user can do all of their analysis from one interface.

4.2.3. Queries in Marvin

Both Marvin Web and Tools provide interfaces for searching the MaNGA data set through a Structured Query Language (SQL)-like interface, either via a web form or a Python class. The Marvin Query system uses a simplified SQL syntax that focuses only on a filter condition using Boolean logic operators and a list of parameters to return. This eliminates the need to learn the full SQL language and the

[114] https://www.sdss.org/dr15/manga/marvin/
[115] https://dr15.sdss.org/marvin
[116] https://sdss-marvin.readthedocs.io/en/stable/
[117] https://www.sdss.org/dr15/manga/manga-target-selection/nsa/
[118] https://sdss-marvin.readthedocs.io/en/stable/installation.html
[119] https://github.com/sdss/marvin

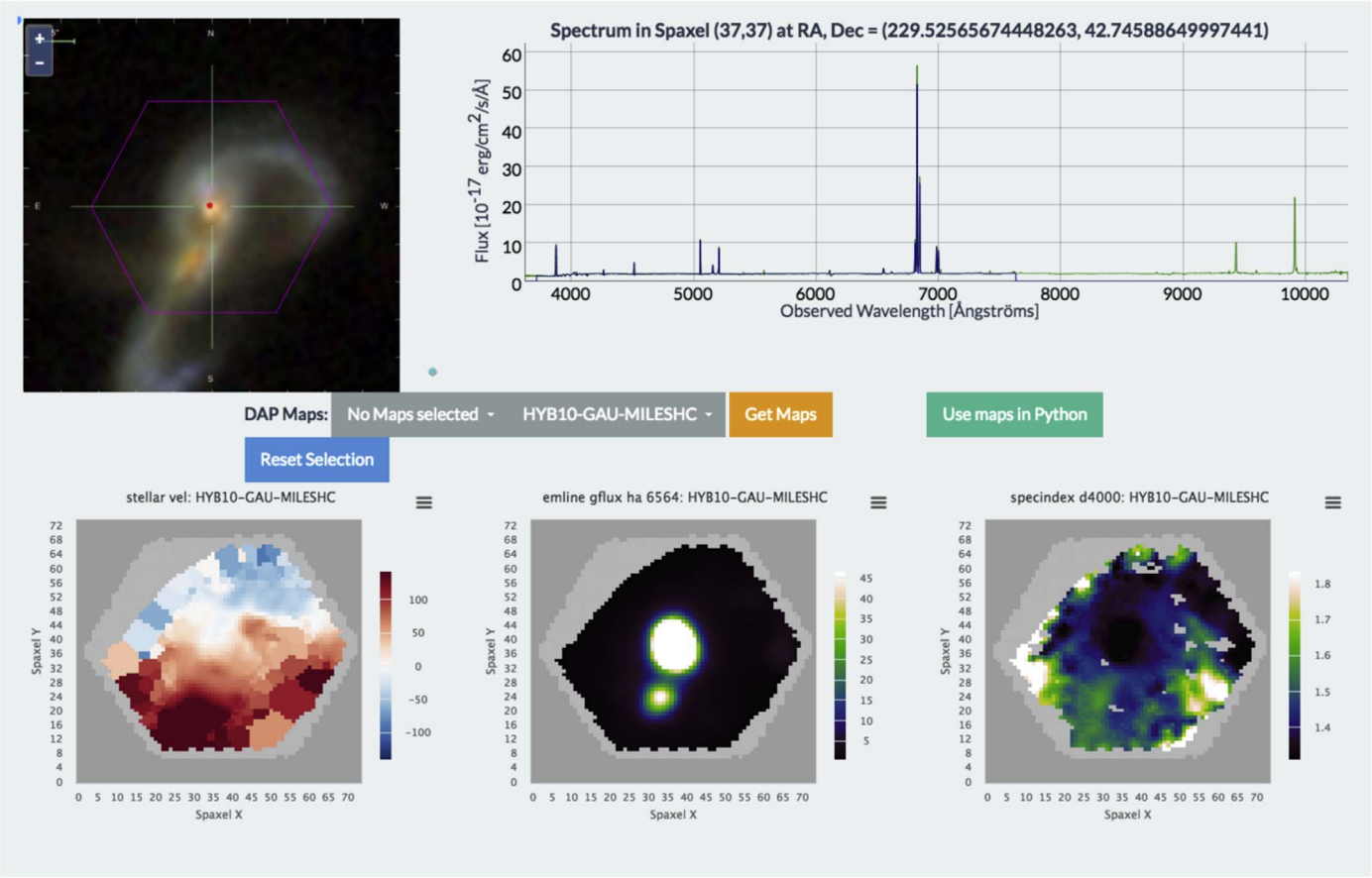

Figure 5. Screenshot of the galaxy maps view of `Marvin Web` for the MaNGA galaxy 12-193481 (Mrk 848). The SDSS three-color image of the galaxy is shown in the top-left part of the figure. The upper-right panel shows the spectrum of the spaxel at the position (37, 37), which corresponds to the center of the bundle (shown by the red dot). The maps show the (lower left) stellar kinematics, (lower middle) Hα emission-line flux, and (lower right) D4000 spectral index for this galaxy based on its unbinned spectral data cube from the MaNGA DAP (see Section 4.1.2).

detailed MaNGA database layout. With this query system, users can make queries across the entire MaNGA sample using traditional global galaxy properties (functionality to perform intragalaxy queries using individual spaxel measurements is planned for a future release). Tutorials for querying with `Marvin` can be found for the web[120] and for the tools.[121]

4.3. MaStar: A Large and Comprehensive Stellar Spectral Library

Stellar spectral libraries are an essential tool for many fields in astronomy. They are especially useful for modeling spectra of external galaxies, including fitting for redshift and stellar kinematics, fitting the continuum to isolate emission lines, and calculating stellar population models (e.g., Leitherer et al. 1999; Bruzual & Charlot 2003; Maraston 2005; Conroy & Gunn 2010; Vazdekis et al. 2010; Conroy 2013) to derive the age, metallicity, and stellar mass of the stellar populations from integrated light spectra. They are also useful for Galactic astronomy and stellar astronomy. Although theoretical spectral libraries have been substantially improved over the years, they are still not realistic enough for certain stellar types (e.g., very cold stars and carbon stars), due to the incomplete line list and difficult-to-model physical effects, such as convection, microturbulence, and deviations from plane-parallel geometry and local thermodynamic equilibrium (non-LTE). Therefore, empirical libraries are still needed for many applications and for calibrating the theoretical models, provided one is able to assign robust stellar parameters to the empirical spectra.

At the beginning of the MaNGA survey, there were no empirical stellar libraries available covering the entire MaNGA wavelength range with a spectral resolution that is equal to or higher than that of MaNGA. Current state-of-the-art empirical stellar libraries also have some other shortcomings. Some libraries have issues with flux calibration or telluric subtraction. Furthermore, all existing libraries have limited stellar parameter space coverage, lacking sufficient sampling in especially cool dwarfs, carbon stars, metal-poor stars, and very hot stars. They also do not sufficiently sample the [α/Fe] versus [Fe/H] space (see Maraston & Strömbäck 2011 for a discussion of all these problems). These issues prompted us to take advantage of a parallel observing opportunity in SDSS-IV for assembling an empirical stellar spectral library that samples a wider stellar parameter space with a larger number of stars than any previous library, and matches MaNGA's wavelength coverage and spectral resolution.

Included in this data release is the first version of the MaNGA Stellar Library (MaStar). These observations are performed by piggybacking on the APOGEE-2N observations during bright time. MaNGA fiber bundles are plugged along with APOGEE fibers into these APOGEE-led plates to observe

[120] https://www.sdss.org/dr15/manga/manga-tutorials/marvin-tutorial/marvin-web/
[121] https://sdss-marvin.readthedocs.io/en/stable/query.html

selected stars. As a result, the MaStar stellar spectra are observed using exactly the same instrument as MaNGA galaxies so they provide an ideal set of templates for modeling stellar continuum and stellar populations in MaNGA galaxies.

The program has so far observed several thousands of stars, each with several epochs of observation. The version we are releasing in DR15 includes 8646 good quality spectra for 3321 unique stars, which cover a wide range in stellar parameter space. The details of the target selection, data reduction, flux calibration, and stellar parameter distribution are described by Yan et al. (2018). Here we provide a brief summary.

4.3.1. Target Selection

Good target selection is essential to achieve wide sampling of the stellar parameter space. We aim to cover the stellar parameter space as completely as possible and sample it roughly evenly. We base our selection primarily on existing stellar parameter catalogs, including APOGEE-1 and -2 (Majewski et al. 2017), SEGUE (Yanny et al. 2009), and LAMOST (Luo et al. 2015). Given the field plan of APOGEE-2, we select all of the stars available in these catalogs in the planned APOGEE-2 footprint. For each star, we count its neighboring stars in stellar parameter space ($T_{\rm eff}$, log g, [Fe/H]) and assign it a selection weight that is inversely proportional to its number of neighbors. The number of APOGEE-2 targeting designs for each field is also taken into account. We then draw our targets randomly in proportion to the normalized selection weight. This method flattens the stellar parameter space distribution and picks rare stars in those fields where they are available.

In fields without stars with known stellar parameters, we use spectral energy distribution (SED) fitting to search for hot and cool stars to patch the stellar parameter distribution at the hot and cool ends.

The targets are required to have g- or i-band magnitude brighter than 17.5 in order to achieve an S/N greater than 50 per pixel in 3 hr of integration, although not all fields have the same integration time or the same number of visits. They are also required to be fainter than 12.7 mag in both g- and i-bands in order to stay below the saturation limit of the detector for 15 minute exposures. We later lowered the saturation limit to 11.7 to include more luminous stars, with a slight offset in fiber placement for stars with magnitudes between 11.7 and 12.7. This slight offset does not affect our flux calibration due to our unique calibration procedure.

These magnitude limits yield relatively few OB stars and blue supergiants, as they have to be very distant or very extincted to fall within this magnitude range. Therefore, we are currently adjusting our exposure time in certain fields to expand our parameter space distribution in the blue and luminous end. The first version of the library does not have many such stars, but we will improve on this for the final version, which we expect to come out in the final SDSS-IV Data Release.

4.3.2. Observations

Observations for MaStar are obtained in a similar fashion to the MaNGA observations except that they are conducted under bright time and without dithering. Since we are piggybacking on APOGEE-2, if APOGEE-2 visits a field multiple times, we would obtain multiple visits for the stars on that plate as well. Therefore, some stars have many visits and some stars have only one visit. Each visit of APOGEE-2 is typically 67 minutes long, which would allow us to take four 15 minute exposures, unless interrupted by weather or other reasons. Each plate has 17 science targets and 12 standard stars, same as MaNGA. We take flat and arc frames before each visit.

4.3.3. Data Reduction

The reduction of the MaStar data is handled by the MaNGA DRP (see Section 4.1.1, Law et al. 2016). It has two stages. The first stage processes the raw calibration frames and science frames to produce the sky-subtracted, flux-calibrated, camera-combined spectra for each fiber in each exposure. The second stage differs between MaNGA galaxy data and MaStar stellar data. For MaStar stellar data, we evaluate the flux ratios among fibers in a bundle as a function of wavelength and constrain the exact location of the star relative to the fiber positions. This procedure helps us derive the light loss due to the finite fiber aperture as a function of wavelength. This procedure takes into account the profile of the PSF and the differential atmosphere refraction. It is similar to how we handle flux calibration in MaNGA data (Yan et al. 2016b). We then correct the spectra for this aperture-induced light loss and arrive at the final flux-calibrated stellar spectra. Comparison with photometry shows that our relative flux calibration are accurate to 5% between the g- and r-bands, and to 3% between r and i, and between the i and z bands.

For each star, we combine the spectra from multiple exposures on the same night and refer to these combined spectra as "visit spectra." We do not combine spectra from different nights together for the same star, because they can have different instrumental resolution vectors and some stars could be variable stars. By summer 2017, we have obtained 17,309 visit spectra for 6042 unique stars. Because not all visit spectra are of high quality, as we will discuss below, we selected only those with high quality and present this subset as the primary set to be released. The primary set contains 8646 visit spectra for 3321 unique stars.

The final spectra are not corrected for foreground dust extinction. Users should make these corrections before using them.

4.3.4. Quality Control

A stellar library requires strict quality control. We have a number of quality assessments carried out in the pipeline to flag poor-quality spectra. We identify cases having low S/N, bad sky subtraction, high scattered light, low PSF-covering fraction, uncertain radial velocity (RV) measurement, and/or those with problematic flux calibration. Each spectrum we release has an associated quality bitmask (`MJDQUAL` for each visit spectrum) giving these quality information. We provide a summary of these in Table 3 and describe them in more detail here.

A large fraction of the observed stars have problematic flux calibration due to the fact that the standard stars on those plates have much less extinction than given by the Schlegel et al. (1998, SFD) dust map. In the flux-calibration step of the MaNGA pipeline, we assume that the standard stars are behind the Galactic dust, and we compare the observed spectra of the standard stars with the dust-extincted theoretical models to derive the instrument throughput curve. This assumption is valid for all galaxy plates that are at high Galactic latitude and

Table 3
Quality Control Bits MJDQUAL for MaStar. See Section 4.3.4 for a Full Explanation

Bit	Description
1	Problematic sky subtraction
2	High scattered light in the raw frame
4	Low PSF-covering fraction
5	Poor flux calibration
6	Unreliable radial velocity estimates
7	Flagged as unreliable from visual inspection
8	Strong emission lines
9	Low S/N

have relatively faint standard stars, placing them at a safe distance behind most of the dust. However, this assumption fails for many fields targeted by MaStar, which are at low Galactic latitudes. Stars at low Galactic latitude are quite likely to be found in front of some fraction of the dust in that direction. Thus, when applying the extinction given by SFD, we overly redden the theoretical models and arrive at an incorrect flux calibration for these fields. We have a solution to this problem, which will be incorporated into the MaStar pipeline in the future. In the current release, the spectra for these stars are just flagged as having poor flux calibration (bit 5 of MJDQUAL).

A significant fraction of the spectra also have unreliable RV estimates. We used a rather limited set of templates in our derivation of the RVs. Thus, stars with very hot or very cool effective temperature, and those with very high and low surface gravity, are more likely to be affected by this issue. These can be identified by checking bit 6 of the MJDQUAL bitmask. All spectra are shifted to the rest frame according to the reported heliocentric RV, regardless of whether the measurement is robust or not.

In addition to these automated checks, we carried out a visual inspection campaign to ensure the quality of each spectrum. Using the Zooniverse Project Builder interface,[122] we started a private project for visually inspecting the spectra. A total of 28 volunteers from within the collaboration participated in the campaign; 10,797 visit spectra were inspected, each by at least three volunteers, to check for issues in flux calibration, sky subtraction, telluric subtraction, emission lines, etc. The results are input to the DRP to assign the final quality flags.

The primary set of spectra we are releasing contains only those spectra that are deemed to have sufficient quality to be useful. We have excluded from the primary set those spectra with problematic sky subtraction (bit 1 of MJDQUAL), low PSF-covering fraction (bit 4), poor flux calibration (bit 5), or low S/N (bit 9), and those identified as problematic by visual inspection (bit 7). The primary set still contains spectra with unreliable heliocentric velocity measurements (bit 6), whose spectra would still be in the observed frame. It also contains spectra with strong emission lines (bit 8), some of which are intrinsic to the star. In addition, stars flagged to have high scattered light in the raw frame (bit 2) are also included as they may not be affected significantly. Other bits that are not mentioned above were never set in the current data release. The users are strongly advised to check the quality flags when using the spectra. Detailed information about the quality flags can be found in Yan et al. (2018).

In addition to these basic quality checks, we are testing the spectra by running them through a population synthesis code (Maraston 2005). This procedure, which will be described in C. Maraston et al. (2019, in preparation), allows us to test the total effect of the goodness of the spectra plus assigned stellar parameters and will be crucial for the joint calculation of stellar parameters and stellar population models. Relevant to this description, this method allows us to spot bad or highly extincted spectra.

4.3.5. Stellar Parameter Distribution

Robust assignment of stellar parameters to the stars are also critical for the stellar library. Our targets are selected from heterogeneous sources. Those selected from APOGEE, SEGUE, and LAMOST have parameters available from their respective catalogs. However, they are measured with different methods and may not be consistent with each other. They also have different boundaries applied in the determination of the parameters. For our target selection purposes, we have made small constant corrections to the parameters to remove the overall systematic difference. These slightly adjusted parameters are included in the catalog we release. However, the corrections are done independent of detailed stellar types. As a result, the parameters from different catalogs can still have subtle stellar-type-dependent systematic differences. For individual stars, they could be used to determine the rough stellar type. But for the library as a whole, we caution against using these input parameters to compare the stars or to construct stellar population models with them.

We are still in the process of determining stellar parameters for all stars in the MaStar library in a way that is as homogeneous as possible. This is not an easy task, because for stars with different stellar types, we need to rely on different spectral features and different methodologies. Although these are not yet available in this version of the library, we present here the extinction-corrected Hertzsprung–Russell (HR) diagram for our stars using photometry and parallax from *Gaia* DR2 (Evans et al. 2018; Gaia Collaboration et al. 2018) and *Gaia*-parallax-based distance estimates from Bailer-Jones et al. (2018). This provides a rough idea of our stellar parameter coverage. Here we only plot stars that are either in directions with a total $E(B-V)$ less than 0.1 mag or more than 300 pc above or below the Milky Way midplane so that we can use the total amount of dust measured by Schlegel et al. (1998) for the extinction correction reliably. The photometry of our targets also come from various sources, including PanSTARRS1 (Chambers et al. 2016), APASS,[123] SDSS, *Gaia* DR1 (Gaia Collaboration et al. 2016), and Tycho-2 (Høg et al. 2000) for a few stars. For stars with PanSTARRS1 photometry, we converted them to SDSS using the formula provided by Finkbeiner et al. (2016). For APASS, we assumed that they are in SDSS filters already. For all of the other non-SDSS stars, we use *Gaia* DR2 photometry to derive the magnitudes in SDSS *gri* bands according to the conversion given by Evans et al. (2018). In Figure 6, we show the *r*-band absolute magnitude (M_r) versus $g-i$ for these stars. The color-coding is based on our preliminary measurement of metallicity using the ULySS

[122] https://www.zooniverse.org/lab

[123] https://www.aavso.org/apass

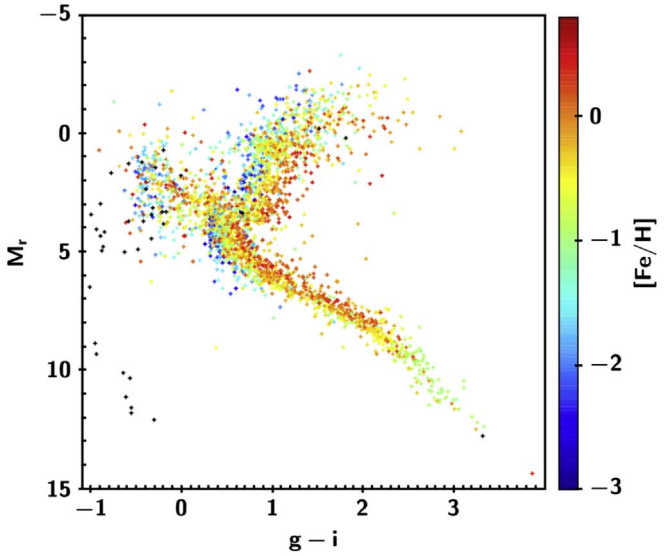

Figure 6. Extinction-corrected HR diagram for MaStar targets, color-coded by our preliminary measurement of metallicity. The *g*-, *r*-, and *i*-bands are in the SDSS photometry system. The absolute magnitudes are derived using parallax-based distance estimates from Bailer-Jones et al. (2018). Only stars for which we are able to get an approximate extinction correction are included here. This figure is reproduced from Yan et al. (2018).

pipeline (Koleva et al. 2009, 2011) with MILES (Sánchez-Blázquez et al. 2006) as the training set.

From Figure 6, we can see that the current released subset of the MaStar library already has a very good coverage across the HR diagram for a wide range of metallicities. But there is significant room for improvement. We need to cover more stars at the luminous end of the red giant branch (RGB) and at the blue end of the main sequence. These will be added in future versions of the library.

4.3.6. Data Access and Usage Information

The MaStar data for this release can be found in two main files: the "`mastarall`" and the "`mastar-goodspec`" files. Both files can be found on the SAS (https://dr15.sdss.org/sas/dr15/manga/spectro/mastar/v2_4_3/v1_0_2/, with data models at https://internal.sdss.org/dr15/datamodel/files/MANGA_SPECTRO_MASTAR/DRPVER/MPROCVER/.

The "`mastarall`" file contains four summary tables of the basic information about the stars and of the information about one or more of their visits. They include the identifier (MaNGAID), astrometry, photometry, targeting bitmask indicating source of photometry, input stellar parameters, plate, IFU, modified Julian date of the visit, derived heliocentric velocity, and spectral quality information. MaNGAID is the identifier to identify unique stars, except in a few cases where the same star was assigned two different MaNGAIDs. These are documented in detail online and in Yan et al. (2018).

The "`mastar-goodspec`" file contains the primary set of high-quality visit spectra. In addition to identification information, we provide the wavelength, flux, inverse variance, mask, spectral resolution vector, and the spectral quality bitmask.

MaStar spectra can also be visualized in SAW (see Section 3 for details).

Table 4
Summary of MaNGA Ancillary Programs with Data in DR15

Ancillary Program	Observed[a]	BITNAME	Binary Digit
Luminous AGNs	25[c]	AGN_BAT	1
		AGN_OIII	2
		AGN_WISE	3
		AGN_PALOMAR	4
Void Galaxies	3	VOID	5
Edge-On Star-forming Galaxies	20	EDGE_ON_WINDS	6
Close Pairs and Mergers	57[d]	PAIR_ENLARGE	7
		PAIR_RECENTER	8
		PAIR_SIM	9
		PAIR_2IFU	10
Writing MaNGA (public outreach)	1	LETTERS	11
Massive Nearby Galaxies	23	MASSIVE	12
Milky Way Analogs	4	MWA	13
	0	MW_ANALOG	23
Dwarf Galaxies in MaNGA	22	DWARF	14
Brightest Cluster Galaxies	24	BCG	17
MaNGA Resolved Stellar Populations	1	ANGST	18
Coma	68	DEEP_COMA	19
IC 342	50	IC 342	20
M31	18	M31	21
SN Ia Hosts	1	SN1A_HOST	26

Notes.
[a] These are bundle counts, not always unique galaxies.
[b] Count for 1, 2, 3, 4 combined.
[c] Count for 7, 8, 9, 10 combined.

4.4. Other Ancillary Programs

We refer the reader to the DR13 paper (Albareti et al. 2017) for the most complete list of MaNGA ancillary programs.[124] These approved programs make use of ∼5% of the MaNGA bundles, and we provide in Table 4 an updated list of the number of bundles available in each documented sample.

There are three new ancillary programs for DR15. These provide observations in the fields of IC 342 and M31 as well as data for a selection of SN1a hosts (`MANGA TARGET3` target bits 20, 21, and 26, respectively).

The IC 342 program will uniformly mosaic the disk of IC 342 using 61 plates, following an initial pilot program of three plates that target individual H II regions across the disk. This galaxy serves as a local reference with 30 pc resolution that can inform our understanding of the unresolved physics in the ∼1 kpc resolution main MaNGA survey.

The M31 ancillary program targets regions in M31 where the underlying physical properties are well constrained from resolved stellar population analyses, provided by the Panchromatic Hubble Andromeda Treasury (PHAT; Dalcanton et al. 2012). The MaNGA observations include 18 regions (50–100 pc in size) that sample a wide range of environmental conditions, including ancient and recent star formation history, dust column, dust geometry, and metallicity. These observations provide a link between resolved stellar populations and

[124] Also see http://www.sdss.org/dr15/manga/manga-target-selection/ancillary-targets.

the inferred properties of unresolved stellar populations, and can be used to assess the ability of spectral fitting codes to recover key physical parameters.

The SN Ia Hosts ancillary program will observe SN Ia host galaxies to investigate causes of the intrinsic variation of SNe Ia. SNe Ia show a spread in absolute magnitude, but can be standardized by taking into account relationships like luminosity-decline rate and SN Ia color to reduce the spread to 0.12 mag. Research over the past several years indicates that some of this remaining spread correlates with global host galaxy properties such as stellar mass, star formation history, and metallicity (e.g., Lampeitl et al. 2010; Gupta et al. 2011; Hayden et al. 2013; Rigault et al. 2013), causing concerns about biases in cosmological measurements. This project will obtain MaNGA data for roughly 40 SN Ia host galaxies in order to look for correlations with SN Ia peak absolute magnitude and host galaxy properties like metallicity and star formation rate averaged over the whole galaxy and at the location of the SN Ia.

DR15 also incorporates a second Milky Way Analogs program (target bit 23), which is similar to the existing program described in DR13, but uses morphological information, rather than star formation rates, in combination with galactic stellar mass to select analogs.

4.5. Value Added Catalogs

As was the case previously in DR14, there are a large number of VACs linked to MaNGA data released in DR15. These either represent additional processing of DRP or DAP output, or follow-up programs or other data useful in combination with MaNGA data. We summarize new or updated VACs below.

4.5.1. Spectral Modeling

In DR15, there are new releases for both the `FIREFLY` (Goddard et al. 2017a) and `Pipe3D` (Sánchez et al. 2016) stellar population modeling and emission-line analysis VACs. Full details of both can be found in the DR14 paper (and references therein), so we give only updates specific to this DR15 release version below.

For DR15, `Pipe3D` version 2.4.3 was run over the MaNGA DR15 data set. The main difference with respect to version 2.1.2 (used in DR14), besides the number of analyzed galaxies, was to solve a bug in the derivation of the equivalent widths of the analyzed emission lines. The current `Pipe3D` VAC provides two different types of data products: (1) a catalog comprising 94 different parameters measured for each of the 4660 galaxies (all galaxies in MaNGA cubes for which `Pipe3D` was able to derive the main stellar population, emission-line, and kinematics properties), and (2) a set of 4660 data cubes `manga.Pipe3D.cube.fits` presenting a set of spatially resolved parameters. The parameters are the same as they were in the DR14 version (Sánchez et al. 2018). More details are available on the data release website, https://www.sdss.org/dr15/manga/manga-data/manga-pipe3d-value-added-catalog/.

The major update to `FIREFLY` with respect to DR14 is the extension of the stellar population modeling grid based on the models of Maraston & Strömbäck (2011). The new catalog uses a finer metallicity grid with the following grid values: [Z/H] = −2.3, −1.9, −1.6, −1.2, −0.9, −0.6, −0.3, 0.0, and 0.3. The new version of the VAC also provides geometrical information so that maps can be produced directly from the VAC (a Python plotting routine is available from the data release website). The entire VAC is available as either a single FITS file containing all measurements or smaller FITS files with selected subsets of the derived parameters. More detail on the catalog is provided on the data release website, https://www.sdss.org/dr15/manga/manga-data/manga-firefly-value-added-catalog/, and in Goddard et al. (2017a) and Parikh et al. (2018).

4.5.2. Morphology and Photometry of MaNGA Targets

As part of DR15, we release one photometry VAC and two morphology VACs.

The `PyMorph` catalog provides photometric parameters obtained from Sérsic and Sérsic+Exponential fits to the 2D surface brightness profiles of the MaNGA DR15 galaxy sample. It uses the `PyMorph` algorithm, which has been extensively tested, to determine the fits (Meert et al. 2013; Bernardi et al. 2017; Fischer et al. 2017), and `PyMorph` reductions of SDSS DR7 galaxies (Abazajian et al. 2009) are available (the UPenn SDSS PhotDec Catalog; Meert et al. 2015, 2016). We have re-run `PyMorph` for all galaxies in the MaNGA DR15 sample. These re-runs incorporate three improvements: they use the SDSS DR14 images, improved bulge-to-disk decomposition by slightly modifying our criteria when using `PyMorph` (see Fischer et al. 2018. for details), and all of the fits in this catalog have been visually inspected for additional reliability (we recommend using "`flag_fit`"). The catalog contains these fits for the *g*-, *r*-, and *i*-bands. One important caveat to note is that position angles (PAs) are reported relative to the SDSS imaging camera columns, which are not aligned with north, so a correction is needed to convert to true PAs. To convert to the usual convention, where north is up, east is left (note that the MaNGA data cubes have north up, east right) set $PA_{MaNGA} = 90^{\circ} - PA_{PyMorph} - PA_{SDSS}$, where $PA_{PyMorph}$ is the value given in this catalog, and PA_{SDSS} is the SDSS camera column position angle with respect to north.

A curated version of the Galaxy Zoo crowdsourced classifications containing an entry for all MaNGA target galaxies is released in DR15. This catalog contains galaxy classifications previously released in Willett et al. (20013, which was selected from the SDSS DR7 galaxy catalog), as well as new unpublished classifications for MaNGA targets missing from that list. All morphological identifications are provided based on the citizen scientist input using the improved technique for aggregation and debiasing described in Hart et al. (2016). This accounts better for redshift bias in the detailed classifications of spiral arms, bars than the version used in Willett et al. (2013). For a simple conversion between Galaxy Zoo classifications and modern (bulge-sized based) T-types, see details in Willett et al. (2013), which also includes general advice on how to best use Galaxy Zoo classifications for science.

A second morphology catalog that has been obtained with the help of "Deep Learning" models is provided. The models were trained (making use of Galaxy Zoo morphologies, as well as morphologies from Nair & Abraham 2010) and tested on SDSS DR7 images (Domínguez Sánchez et al. 2018). The morphological catalog contains a series of Galaxy-Zoo-like attributes (edge-on, barred, bulge prominence and roundness),

as well as a T-Type and a finer separation between pure elliptical and S0 galaxies.

4.5.3. H I-MaNGA—H I 21 cm Follow-up for MaNGA

The first data release of "H I-MaNGA," the H I follow-up project for MaNGA, is provided as a VAC in DR15. This follow-up program is presented in Masters et al. (2018) and is the result of single-dish radio 21 cm H I observations of MaNGA galaxies using the Robert C. Byrd Green Bank Telescope (GBT). The depth of this observing is aimed to be similar to the Arecibo Legacy Fast Arecibo L-band Feed Array (ALFALFA) blind H I survey (Haynes et al. 2018), which covers some of the MaNGA footprint (see Figure 2), with a goal of enabling studies to use H I data from both surveys. In this first release, data are provided for 331 MaNGA galaxies observed in the 2016 GBT observing seasons under project code `AGBT16A_95`. Total H I masses and line widths (measured with five different common techniques) are provided for all detections, while H I mass upper limits (assuming a line width of 200 km s^{-1}) are provided for non-detections. H I-MaNGA has observed an additional ∼2000 MaNGA galaxies in the 2017 observing season (under project code `AGBT17A_12`); these data will be released in a future VAC. The sky distribution of all MaNGA galaxies observed by this program is shown in Figure 2.

4.5.4. GEMA-VAC; Galaxy Environment for MaNGA VAC

The environment in which a galaxy resides plays an important role in its formation and evolution. Galaxies evolve as a result of intrinsic processes (i.e., their nature—this includes processes such as internal secular evolution, feedback of various kinds etc.), but they are also exposed to the influences of their local and large-scale environments (i.e., how they are "nurtured"). We present the Galaxy Environment for MaNGA Value Added Catalog (GEMA-VAC), which provides a quantification of the local and large-scale environments of all MaNGA galaxies in DR15. There are many different definitions of environment, and there are also several ongoing projects within the MaNGA team exploring the influence the environment has on galaxy properties. With this VAC, we aim to join and coordinate efforts so that the entire astronomical community can benefit from the products. The GEMA-VAC catalog will be described in more detail in M. Argudo-Fernández et al. (2019, in preparation). We describe the contents of the VAC briefly below.

We estimate the tidal strength parameter for MaNGA galaxies in pairs/mergers (B. Hsieh et al. 2019, in preparation), the tidal strengths exerted by galaxies in the catalog of galaxy groups in Yang et al. (2007), and tidal forces exerted by nearby galaxies in two different fixed-aperture volume-limited samples (namely 1 and 5 Mpc projected distances within a line-of-sight velocity difference of $\Delta v \leqslant 500$ km s^{-1}; Argudo-Fernández et al. 2015). Estimations of the local densities with the distance to the fifth nearest neighbor are also provided. The local density within the N nearest neighbors includes the corrections explained in Goddard et al. (2017b) following the methodology described in Etherington & Thomas (2015). To have a more general picture of the environment, we also provide a characterization of the cosmic web environment, which can be used to identify galaxies in clusters, filaments, sheets, or voids, as explained in Zheng et al. (2017). The full details of the reconstruction of these density and tidal fields are described in Wang et al. (2009, 2012).

4.5.5. MaNGA Spectroscopic Redshifts

We present a VAC that contains the best-fit spectroscopic redshift and corresponding model flux for each MaNGA spectrum that has sufficient S/N. We provide the mean of the spectroscopic redshifts sampled within the inner high-S/N region of the MaNGA galaxies, which can be compared to the single-valued NSA catalog redshift. Since the MaNGA instrument uses the BOSS spectrograph, our results are derived by iterative application of the BOSS pipeline's spec1d software (Bolton et al. 2012) to precisely measure the redshift using the higher S/N measurements as a prior to the algorithm, which allows us to determine good redshifts on spectra that would not otherwise have sufficient S/N to result in a good redshift. Since the MaNGA survey uses an IFU, the RV profile of the galaxy can significantly impact the redshift of each spectra. Thus, the spectroscopic redshifts can both be a benefit to galaxy kinematic measurements and improve the accuracy of spectra modeling and analysis. The authors of this VAC have used the spectroscopic redshifts to search for background emission lines to discover strong gravitational lenses in MaNGA (Talbot et al. 2018).

5. Other Survey Data and Products

5.1. APOGEE-2

SDSS DR15 includes no new APOGEE data. The currently available set of APOGEE Survey data consists of the first two years of SDSS-IV APOGEE-2 (2014 July–2016 July) as well as the entirety of SDSS-III APOGEE-1 (2011 August–2014 July) and is an exact duplicate of that data, which was released in DR14. DR15-associated APOGEE documentation builds upon that from DR14, with extended explanations and the addition of information and relevant text (e.g., a description of the New Mexico State University (NMSU) 1.0 m Telescope). Note that the DR15 APOGEE data model has remained largely the same with only slight revisions to the text for clarity. Described below are the APOGEE technical papers that contain details which should assist users in the exploitation of APOGEE data as well as provide further understanding as to data quality (Zasowski et al. 2017; Holtzman et al. 2018; Jönsson et al. 2018; Pinsonneault et al. 2018; Wilson et al. 2018). Additionally, details are provided on the recently generated VAC from Donor et al. (2018), which contains a catalog of identified APOGEE open cluster members. There are currently four VACs that rely upon APOGEE DR14 in order to extend and enhance the standard APOGEE data release products (DR14 APOGEE TGAS Catalog, APOGEE Red Clump Catalog, APOGEE DR14 Based Distance Estimations, and OCCAM).[125]

5.1.1. Technical Papers

Two new APOGEE-related technical papers are highlighted below: the instrument paper from Wilson et al. (2018), which relays an extensive description of the APOGEE spectrographs,

[125] More information regarding all available APOGEE VACs including brief descriptions and the corresponding authors may be found in the SDSS online documentation (http://www.sdss.org/dr15/data_access/value-added-catalogs/).

and the APOKASC paper from Pinsonneault et al. (2018), which details the APOGEE spectroscopic follow-up of *Kepler* stars.

APOGEE Instrument Paper. The publication from Wilson et al. (2018) describes the design and performance of the near-infrared, fiber-fed, multiobject, high-resolution APOGEE spectrographs. The first APOGEE instrument has been in operation on the 2.5 m Sloan Telescope at the Apache Point Observatory in New Mexico, USA, since 2011 (a northern hemisphere site). Several key innovations were made during the development of the APOGEE instrument, which include a multifiber connection system known as a "gang connector," which allows for the simultaneous disconnection and reconnection of 300 fibers; hermetically sealed feedthroughs to permit fibers to pass through the cryostat wall continuously; the first cryogenically deployed mosaic volume phase holographic grating; and a massive refractive camera that comprising large-diameter monocrystalline silicon and fused silica elements. Specifically for the northern spectrograph, Wilson et al. (2018) report on the following: the performance of the 2.5 m Sloan Foundation Telescope in the near-infrared wavelength regime, the cartridge and fiber systems, the optical and optomechanical systems, the detector arrays and electronic controls, the cryostat, the instrument control system, calibration procedures, instrument optical performance and stability, and lessons learned. The final sections of Wilson et al. (2018) provide similar details on the second APOGEE spectrograph located at the 2.5 m du Pont Telescope at LCO in Chile. This second (southern hemisphere-based) instrument, a close copy of the first, has been operating since 2017 April. Wilson et al. also contains multiple appendices for the interested user.

The Second APOKASC Catalog. Over both the APOGEE-1 and APOGEE-2 Surveys, a joint effort known as the APOGEE *Kepler* Asteroseismic Science Consortium (APOKASC), APOGEE has engaged in a spectroscopic follow-up of stars in the *Kepler* field. Pinsonneault et al. (submitted) present the second APOKASC Catalog of stellar properties for a sample of 6681 evolved stars with APOGEE spectroscopic parameters and *Kepler* asteroseismic data analyzed using five independent techniques. The APOKASC data include the evolutionary state, surface gravity, mean density, mass, radius, and age, and the spectroscopic and asteroseismic measurements used to derive them. As shown in Figure 7, the APOKASC catalog asteroseismic log g values and evolutionary state classifications allow for a clear distinction between RGB and red clump (RC) members. Pinsonneault et al. (2018) employ a new empirical approach for combining asteroseismic measurements from different methods, calibrating the inferred stellar parameters, and estimating uncertainties. With high statistical significance, they find that asteroseismic parameters inferred from the different pipelines have systematic offsets that are not removed by accounting for the differences in their solar reference values. Pinsonneault el al. include theoretically motivated corrections to the large frequency spacing ($\Delta\nu$) scaling relation as well as calibrates the zero point of the frequency of maximum power ($\nu_{\rm max}$) relation to be consistent with masses and radii for members of star clusters. For most targets, the parameters returned by different pipelines are in much better agreement than would be expected from the pipeline-predicted random errors, but 22% of them had at least one method not return a result and a much larger measurement dispersion. This supports the usage of multiple analysis techniques for asteroseismic stellar population studies.

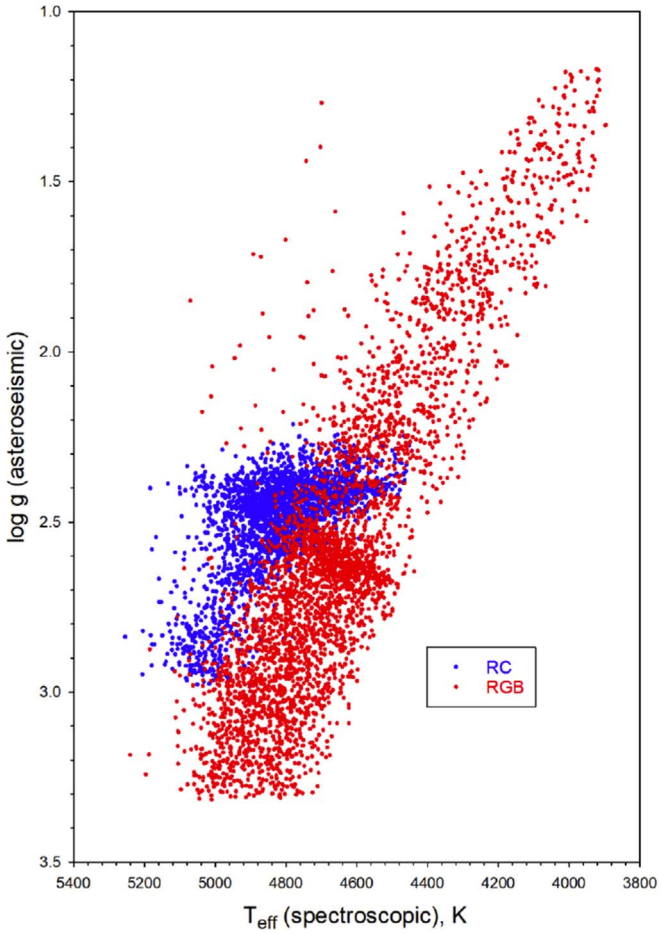

Figure 7. Spectroscopic effective temperature (from APOGEE DR14) vs. asteroseismic surface gravity (log g) in the APOKASC sample by asteroseismic evolutionary state. Red clump (RC; core He-burning) stars are signified in blue while red giant branch (RGB; H-shell or double shell burning) stars are shown in red. The two populations have a clear offset in this plot, with RC stars having higher surface gravity at the same temperature compared to RGB stars.

In the SDSS DR14 data release paper (Abolfathi et al. 2018), brief references were made to the Holtzman et al. (2018) and Jönsson et al. (2018) publications. For the benefit of users, concise descriptions of each are now provided. Please note that in addition to the DR15 documentation, users should refer to these publications for detailed information regarding the Data Reduction Pipeline (DRP) and the APOGEE Stellar Parameter and Chemical Abundance Pipeline (ASPCAP), as well as to understand data quality and performance.

SDSS/APOGEE DR13 and DR14 Pipeline Processing and Data Description. Holtzman et al. (2018) describe the data and analysis methodology used for the SDSS/APOGEE Data Releases 13 and 14, as well as highlight differences from the DR12 analysis presented in Holtzman et al. (2015). For example, the work demonstrates some improvement in the handling of telluric absorption and persistence in the DR13/DR14 versions of APOGEE-2 data as opposed to DR12. Holtzman et al. (2018) detail the derivation and calibration of stellar parameters, chemical abundances, and respective uncertainties, along with the ranges over which calibration was performed. The work reports some known issues with the public data related to the calibration of the effective

temperatures (DR13), surface gravity (DR13 and DR14), and C and N abundances for dwarfs (DR13 and DR14). Holtzman et al. (2018) also discuss how results from The Cannon (Ness et al. 2015) are included in DR14 and compare those with the values from ASPCAP.

Comparison of SDSS/APOGEE DR13 and DR14 Values to Optical Results. Jönsson et al. (2018) evaluate the ASPCAP performance for both the DR13 and DR14 APOGEE data sets with 160,000 and 270,000 stars, respectively. A comparison of the ASPCAP-derived stellar parameters and abundances to analogous values inferred from optical spectra and analysis with a subset of several hundred stars is done. For most elements, Jönsson et al. (2018) find that the DR14 ASPCAP results have systematic differences with the comparison samples of less than 0.05 dex (median) and random differences of less than 0.15 dex (standard deviation). These departures are attributed to a combination of uncertainties in both the comparison samples as well as the ASPCAP analysis. Specifically, in comparison to the optical data, Jönsson et al. (2018) find that magnesium is the most accurate alpha-element derived by ASPCAP while nickel is the most accurate Fe-peak element (excluding iron).

Additionally, in Abolfathi et al. (2018), detailed information was provided regarding the recently published APOGEE-2 Targeting Paper from Zasowski et al. (2017). Users are encouraged to consult Zasowski et al. for specific details and insight regarding APOGEE-2 targeting.

5.1.2. New VAC—OCCAM

The Open Cluster Chemical Analysis and Mapping (OCCAM) Survey generates a VAC of open cluster members as targeted in both APOGEE-1 and APOGEE-2 fields. To establish membership probabilities, the catalog combines APOGEE DR14 DRP-derived RVs and ASPCAP-derived metallicities with proper motion (PM) data from *Gaia* DR2. This first VAC from the OCCAM Survey includes 19 open clusters, each with four or more APOGEE members. The OCCAM VAC consists of two components: a set of bulk cluster properties, which include motions (RV, PM) as well as robust average element abundance ratios, and a set of membership probabilities for all stars considered in the analysis of the 19 open clusters. For further information on the OCCAM Survey, please consult Donor et al. (2018).

5.2. eBOSS, TDSS, and SPIDERS

There are no new reduced eBOSS data included in this data release; the VACs released are based on previously released eBOSS spectra. The final eBOSS spectroscopic sample will be released in DR16. For more details on what is coming in DR16, see Section 6.1.

DR14 marked the first cosmological sample from eBOSS, consisting of spectra predominantly of luminous red galaxies (LRGs) and quasars. These data enabled the first baryon acoustic oscillation (BAO) measurement in the $1 < z < 2$ redshift range from quasars (Ata et al. 2018) and a 2.6% precision constraint on the distance scale using the clustering of LRGs (Bautista et al. 2018). These measurements reflect the two primary goals for early eBOSS science, yet are only a subset of the results from the two-year eBOSS sample. The large-scale structure catalogs for both of these studies were released in 2018 July and were not described in the 14th Data Release publication. These VACs can now be accessed from the DR14 site[126] and from this new release in a parallel location. These catalogs contain all necessary information such as the window function, systematic quantities, completeness estimates, and corrections for close pairs and redshift failures to reproduce those clustering measurements, similar to the catalogs from the final BOSS sample (Reid et al. 2016).

The publications that document the DR14 target selection algorithms (Myers et al. 2015; Palanque-Delabrouille et al. 2016; Prakash et al. 2016) will also describe the LRG and quasar samples for the final eBOSS sample. Several new algorithms for spectroscopic data reductions were implemented in DR14 (Jensen et al. 2016; Hutchinson et al. 2016); we will further improve sky subtraction with higher order models to the fiber-to-fiber sky model, flux calibration with new models for standard stars, and spectral extraction to account for cross-talk such as that found in Hemler et al. (2018, submitted) for the final sample. A new method to improve the classification of galaxy spectra (Hutchinson et al. 2016) was implemented in DR14, and new methods for classifying emission-line galaxies (ELGs) and quasars are being considered for the final sample.

5.3. Optical Emission-line Properties and Black Hole Mass Estimates for SPIDERS DR14 Quasars

This VAC, released in DR15, contains optical spectral properties for all X-ray-selected SPIDERS quasars released in DR14. The SPIDERS DR14 catalog is based on a clean sample of 9399 sources from the Second *ROSAT* All-Sky Survey catalog (2RXS; Boller et al. 2016) and 1413 sources from the first *XMM-Newton* Slew survey catalog (XMMSL1; Saxton et al. 2008) with optical spectra available. X-ray sources were matched to ALLWISE infrared counterparts using the Bayesian algorithm "NWAY" (Salvato et al. 2018), which were then spectroscopically identified using SDSS (Dwelly et al. 2017). Visual inspection results for each object in this sample are available from a combination of literature sources and the SPIDERS group, which provide both reliable redshifts and source classifications. A spectral fitting code, which fits the spectral regions around the Hβ and MgII emission lines and provides both line and continuum properties, bolometric luminosity estimates, as well as single-epoch black hole mass estimates, has been produced. This VAC includes X-ray flux measurements, visual inspection results, optical spectral properties, black hole mass estimates, and additional derived quantities for all SPIDERS DR14 quasars. For more details, see Coffey et al. (2018).

6. Future Plans

SDSS-IV has a full two years of operations remaining and is planning a further two public data releases. The next data release, DR16, is now scheduled for 2019 December and will comprise data taken by both the APOGEE-N and APOGEE-S instruments through 2018 July as well as being the final complete data release for eBOSS operations. The final, complete release, DR18 (which will follow an internal only DR17) is planned for 2020 December.

[126] https://data.sdss.org/sas/ebosswork/eboss/lss/catalogs/DR14/

6.1. eBOSS

The eBOSS schedule was recently accelerated in order to achieve its cosmological goals earlier than previously planned. This acceleration began on 2018 January 1 and continues through 2019 February 16, at which time eBOSS will complete its program significantly ahead of the start of the Dark Energy Spectroscopic Instrument (DESI) survey (DESI Collaboration et al. 2016). Under the original schedule, eBOSS and MaNGA divided the dark time roughly equally. Under the new schedule, *eBOSS* controlled all of the dark time in 2018 January and February, we returned to the original shared schedule for 2018 March through July, and *eBOSS* controlled all of the dark time in 2018 from August through 2019 February 16.

The final data sample will include the spectra from observations covering 302 ELG plates that define the complete ELG sample following the selection algorithms in Raichoor et al. (2017). The final LRG and quasar samples will cover a volume roughly 2.3 times larger than the two-year cosmology samples released and analyzed in DR14.

The final eBOSS sample will enable precision measurements of BAO in the clustering of galaxies, quasars, and the Lyα forest. The final sample will also enable new measurements of redshift space distortions in the anisotropic clustering of galaxies and quasars over the redshift range $0.6 < z < 2.2$. The next data release has been scheduled around the expected time that these analyses will be completed. This data release will be the last to include new eBOSS data. Also included will be the VACs that will allow others to reproduce the final cosmology measurements.

6.2. SPIDERS

At the completion of the eBOSS survey, SPIDERS will have only obtained spectra from the ongoing follow-up program of *ROSAT* and *XMM-Newton* sources. Continuing at the current pace, at the end of the survey, SPIDERS will have collected about 12,000 new spectra of X-ray-selected AGNs and 40,000 spectra of member galaxies of about 5000 clusters over the final eBOSS area.

The delayed launch of the *eROSITA* satellite (Predehl et al. 2014), combined with the accelerated program for obtaining eBOSS spectra, means that it will not be possible to obtain redshifts for *eROSITA* targets during routine eBOSS operations. The *eROSITA* Performance Verification data set is currently planned to be available by early to mid-2019 and should consist of 120 deg^2, with 100–140 targets per deg^2. To address at least part of the original goals of SPIDERS involving *eROSITA* follow-up, we plan to dedicate a special set of 12 plates for these targets; however, this plan cannot be confirmed until 2019 February.

6.3. TDSS

The accelerated pace for eBOSS discussed above correspondingly accelerates TDSS, which also relies on the BOSS spectrographs, using a small portion (about 5%) of the optical fibers piggybacking on eBOSS plates. TDSS observations will thus effectively also conclude with eBOSS data collection in about 2019 mid-February, and with SDSS-IV/TDSS data to be included in the future DR16. Although all three main components of TDSS—the optical spectroscopic follow-up of PS1 photometric imaging variables (e.g., see Morganson et al. 2015; Ruan et al. 2016), repeat Few-Epoch Spectroscopy (FES) of selected subclasses of stars and quasars anticipated or suspected to reveal spectroscopic variability (e.g., see MacLeod et al. 2018), and the more recently initiated TDSS Repeat Quasar Spectroscopy (RQS; also see MacLeod et al. 2018) program—thereby also have been accelerated toward completion, in practice this advance is such that SDSS-IV data collection for the TDSS RQS program in particular is now nearing completion.[127] The TDSS RQS program obtains multiepoch spectra for thousands of known quasars (and with a larger sample size and greater homogeneity and less a priori bias toward specific quasar subclasses than the TDSS FES programs), all of which have at least one earlier epoch of SDSS spectroscopy already available in the SDSS archive. The RQS program specifically addresses quasar spectral variability on multiyear timescales, and in addition to its own potential for new discoveries of phenomena, such as changing-look quasars or broad absorption line (BAL) variability and others, will also provide a valuable (and timely) resource for planning yet larger scale multiepoch quasar repeat spectral observations anticipated for the Black Hole Mapper program in the future SDSS-V (see Section 6.6 below). From data taken for the RQS SDSS-IV program to date, we expect RQS to add another recent epoch of spectroscopy for ∼16,000 SDSS quasars, sampling across a broad range of properties including redshift, luminosity, and quasar subclass type.

6.4. MaNGA

MaNGA will continue to take observations for the next two years of SDSS-IV operations. The time trade with eBOSS has slowed the rate of observations during 2018; however, it will provide an overall increase in the total observing time allocation for MaNGA by 8%. The projected final survey footprint, assuming we continue nominal survey operations through 2020 July, is shown for two different expectations of weather at the telescope and overlaid on other relevant surveys in Figure 2. We expect to exceed our original goal of 10,000 galaxies slightly under nominal weather conditions.

6.5. APOGEE-2

The APOGEE-2 Survey continues to acquire observations from both the northern and southern hemispheres. SDSS-IV Data Release 16 will contain the first APOGEE-2 data from the southern instrument. For DR16, a variety of improvements are planned to both the DRP and the APOGEE Stellar Parameters and Chemical Abundance Pipeline (ASCAP). A new atomic line list will be generated (which will include transitions of Ce II and Nd II), and a new molecular list will be assembled (which will be more extensive in size and will incorporate FeH features). An expansion of the stellar atmosphere model grid is underway, which will entail the inclusion of higher surface gravities, lower carbon abundances, and higher nitrogen abundances. Note that Model Atmospheres in Radiative and Convective Scheme (MARCS[128]) models (Gustafsson et al. 2008) will be employed for both the M and GK grids, ensuring a smooth transition across an effective temperature range of approximately $T_{\rm eff} = 2500$–6000 K. Additionally, some tweaking of the data processing and derivation procedure will occur. Planned modifications include the improvement of the LSF

[127] This is primarily just because RQS piggybacks on a subset of eBOSS plates, which received recent heavy emphasis.
[128] http://marcs.astro.uu.se

determination (with the potential employment of on-the-fly LSF derivation), a better methodology for the extraction of the individual element abundances, and an improved technique for filling holes in the stellar atmosphere model grid.

6.6. SDSS-V

Preparations for the fifth generation of SDSS are underway, with SDSS-V anticipated to begin operations in 2020 (Kollmeier et al. 2017). SDSS-V will collect data at both APO and LCO using the existing APOGEE and BOSS spectrographs on the 2.5 m telescopes, as well as new optical spectrographs dedicated to IFS on new smaller telescopes. The current SDSS plugplate system will be replaced with robotic fiber positioners in the focal planes of the 2.5 m telescopes.

SDSS-V comprises three primary projects: the Milky Way Mapper, the Black Hole Mapper, and the Local Volume Mapper. The Milky Way Mapper will use the APOGEE and BOSS spectrographs to observe 4–5 million stars in the Milky Way and Local Group, probing questions of galaxy formation and evolution, stellar astrophysics, and stellar system architecture. The Black Hole Mapper will use the BOSS spectrographs to measure masses for ∼1200 supermassive black holes via reverberation mapping (e.g., Grier et al. 2017), determine spectral variability for ∼25,000 quasars, and provide identifications and redshifts for ∼400,000 X-ray sources detected by *eROSITA* (Predehl et al. 2014). The Local Volume Mapper will collect IFS using new, $R \sim 4000$ optical spectrographs coupled to small telescopes at APO and LCO. These spectra will span ∼3000 deg^2 of sky in the Milky Way midplane, the Magellanic Clouds, and other Local Group galaxies at high spatial resolution, with the goal of tracing ISM physics and stellar–ISM energy exchange on different physical scales in a range of galactic environments.

6.7. Long-term Sustainability of the SDSS Archives

Starting in 2017, the Science and Catalog Archive Teams have been proceeding on a roadmap toward a sustainable data archive,[129] designed to protect the legacy of SDSS Data.

Some of the steps on this roadmap, which are currently receiving attention, include:

1. *Archival-quality Storage:* The SAS file system was not designed to last beyond the warranty of the disks, and disk corruption issues require meticulous and time-intensive repairs. The SAS Team is currently implementing a ceph-based archival-quality object storage system (Weil et al. 2006) similar to that used by organizations specializing in big data (e.g., Google and Amazon), providing complete internal redundancy, support for geographical distribution, internal failure detection and self-recovery, and inexpensive backup in cloud-based big data object storage systems.
2. *Science Archive Database:* The census of what is contained on the SAS is managed through a Python system with a database that records the hundreds of millions of file paths, file sizes, and file verification checksums. This system is currently being re-implemented to allow a more seamless and high-speed data access.
3. *Migrating the SDSS Software Repository to GitHub:* The SDSS subversion software repository, currently served alongside the SAS, will be replaced by repositories copied into a GitHub organization (https://github.com/sdss), with GitHub Teams created to manage repository access control, with public release of software including open source licensing, starting with DR15 (e.g., Marvin and the underlying code "Marvin's Brain").
4. *SDSS Software Framework Development:* The Data and Operations Teams are currently designing a new software framework to provide Python-based tools, including improved data access, database access, data model documentation, and machine-readability.
5. *SDSS Software Containers:* Portable images of SDSS systems have been developed and implemented on Docker Hub and are currently used at NERSC for the Science Archive Mirror and JHU for Science Archive Webapp development (e.g., Marvin at JHU). The data team is now looking at developing a new wave of such virtual machines to replicate the experience of working on an SDSS computer at the University of Utah.

6.7.1. Modernizing SkyServer

SkyServer has been the primary online web portal to the CAS since the beginning of SDSS, and although it underwent a significant facelift in 2007, it is now woefully outdated in terms of its layout and user experience, and generally in terms of its usability and accessibility. SkyServer has been due for a rewrite with modern web technology for several years now, and we are finally undertaking this daunting task as we wind down SDSS-IV and look forward to SDSS-V. One of the biggest constraints that makes this a difficult enterprise is the large user base that SkyServer has built over the past 15+ years. We do not want to completely rearrange the site in such a way that users no longer recognize it, and more importantly, we do not want to break all of the functionality that works very well currently in spite of the outdated interface. In short, we want to adopt a philosophy of going from "working to working" versions as we modernize the site. We list below the specific changes we are currently working on.

1. *Upgrade Technology:* First and foremost, we are upgrading the web technology underneath SkyServer. This includes everything from the version of HTML and CSS that it was originally written in, to the way that the SkyServer website code is logically organized. We are going toward the MVC (model–view–controller) paradigm that modern websites use to produce modular, reusable, and robust web applications.
2. *Portability:* SkyServer has been a Microsoft Windows application developed with the .NET framework all along. This has made it very difficult to port even the front end to any other platform. Now, with the availability of .NET Core, we have the opportunity to migrate the website to a portable platform that can not only run in Linux, but can also be Dockerized.
3. *Usability:* Usability standards have changed considerably since the time when SkyServer originally came online. In spite of significant upgrades to different parts of SkyServer over the years, there has not been a comprehensive reexamination of the usability aspects. We aim to rectify this as we redesign the user interface. Usability changes will include the effective presentation of information, compatibility with all browsers,

[129] Funded by a dedicated grant from the Sloan Foundation.

responsiveness of page loads, and consistency of display modes (e.g., opening a new tab for results from a query and/or bringing the results pane to the front).

4. *Accessibility:* Accessibility pertains to the versatility of the website and how responsive and easy it is to use and work with for users that are restricted in various ways. This ranges from users on mobile devices to users with restricted access to the internet as well as users with impaired vision or other handicaps. Incorporating modern web design standards and technologies will mostly take care of these aspects, but we will pay special attention to make sure that SkyServer can be used by as many people as possible anywhere in the world there is internet access.
5. *Integrate SkyServer and Voyages:* SkyServer has an extensive educational section that contains several levels of classroom exercise based on SDSS data. These are known collectively as the SkyServer Projects. Voyages is a SkyServer "spinoff" website that has become quite popular and presents several virtual "voyages" through the SDSS data for non-scientist audiences. The Voyages website is a much more modern web application that is based on a content management system (CMS)—WordPress. This allows new pages and functionality to be added to Voyages much more easily than to SkyServer. As part of the SkyServer modernization, we are migrating all of the SkyServer student projects to Voyages and using the same CMS (WordPress) for SkyServer too. We are also integrating Voyages further with SkyServer so that it uses the SkyServer API to run queries on the SDSS data.
6. *Streamline CAS ⇔ SAS Interface:* There are hooks currently between SkyServer/Voyages and the SAS, but they are awkward at best. The SAS API has recently been upgraded, and the points of access to SAS data that currently exist in SkyServer and Voyages will be updated to use the proper SAS API calls.

These steps will help ensure the availability of SDSS data to astronomers for years to come, and long beyond the current funded plans for SDSS-IV and SDSS-V. The CAS data and access tools will at that point be well positioned to be readily integrated into existing data centers for a minimal incremental cost.

Funding for the Sloan Digital Sky Survey IV has been provided by the Alfred P. Sloan Foundation, the U.S. Department of Energy Office of Science, and the Participating Institutions. SDSS-IV acknowledges support and resources from the Center for High-Performance Computing at the University of Utah. The SDSS website is www.sdss.org.

SDSS-IV is managed by the Astrophysical Research Consortium for the Participating Institutions of the SDSS Collaboration including the Brazilian Participation Group, the Carnegie Institution for Science, Carnegie Mellon University, the Chilean Participation Group, the French Participation Group, Harvard-Smithsonian Center for Astrophysics, Instituto de Astrofísica de Canarias, The Johns Hopkins University, Kavli Institute for the Physics and Mathematics of the Universe (IPMU)/University of Tokyo, Korean Participation Group, Lawrence Berkeley National Laboratory, Leibniz Institut für Astrophysik Potsdam (AIP), Max-Planck-Institut für Astronomie (MPIA Heidelberg), Max-Planck-Institut für Astrophysik (MPA Garching), Max-Planck-Institut für Extraterrestrische Physik (MPE), National Astronomical Observatories of China, New Mexico State University, New York University, University of Notre Dame, Observatário Nacional/MCTI, The Ohio State University, Pennsylvania State University, Shanghai Astronomical Observatory, United Kingdom Participation Group, Universidad Nacional Autónoma de México, University of Arizona, University of Colorado Boulder, University of Oxford, University of Portsmouth, University of Utah, University of Virginia, University of Washington, University of Wisconsin, Vanderbilt University, and Yale University.

This publication uses data generated via the Zooniverse.org platform, development of which is funded by generous support, including a Global Impact Award from Google, and by a grant from the Alfred P. Sloan Foundation.

This research was made possible through the use of the AAVSO Photometric All-Sky Survey (APASS), funded by the Robert Martin Ayers Sciences Fund.

The PanSTARRS1 Surveys (PS1) and the PS1 public science archive have been made possible through contributions by the Institute for Astronomy, the University of Hawaii, the Pan-STARRS Project Office, the Max-Planck Society and its participating institutes, the Max Planck Institute for Astronomy, Heidelberg, and the Max Planck Institute for Extraterrestrial Physics, Garching, The Johns Hopkins University, Durham University, the University of Edinburgh, the Queen's University Belfast, the Harvard-Smithsonian Center for Astrophysics, the Las Cumbres Observatory Global Telescope Network Incorporated, the National Central University of Taiwan, the Space Telescope Science Institute, the National Aeronautics and Space Administration under grant No. NNX08AR22G issued through the Planetary Science Division of the NASA Science Mission Directorate, the National Science Foundation grant No. AST-1238877, the University of Maryland, Eötvös Loránd University (ELTE), the Los Alamos National Laboratory, and the Gordon and Betty Moore Foundation.

This work presents results from the European Space Agency (ESA) space mission *Gaia*. *Gaia* data are being processed by the *Gaia* Data Processing and Analysis Consortium (DPAC). Funding for the DPAC is provided by national institutions, in particular the institutions participating in the *Gaia* MultiLateral Agreement (MLA). The *Gaia* mission website is https://www.cosmos.esa.int/gaia. The *Gaia* archive website is https://archives.esac.esa.int/gaia.

We would like to thank the e-Science Institute at the University of Washington, Seattle, for their hospitality during DocuVana 2018. This event held in 2018 May kickstarted the documentation for DR15 (including this paper) and was organized by Jennifer Sobeck and José Sánchez-Gallego and Anne-Marie Weijmans and attended by Amy Jones, Ben Murphy, Bonnie Souter, Brian Cherinka, David Stark, David Law, Dan Lazarz, Gail Zasowski, Joel Brownstein, Jordan Raddick, Julie Imig, Karen Masters, Kyle Westfall, Maria Argudo-Fernández, Michael Talbot, Rachael Beaton, Renbin Yan, and Sten Hasselquist (as well as Becky Smethurst, Rita Tojeiro, Ben Weaver, and Ani Thaker via video link).

This research made use of ASTROPY, a community-developed core PYTHON (http://www.python.org) package for Astronomy (Robitaille et al. 2013); IPYTHON (Pérez & Granger 2007), MATPLOTLIB (Hunter 2007), NUMPY (van der Walt et al. 2011), SCIPY (Jones et al. 2001), and TOPCAT (Taylor 2005).

ORCID iDs

Brett H. Andrews https://orcid.org/0000-0001-8085-5890
Vladimir Avila-Reese https://orcid.org/0000-0002-3461-2342
Carles Badenes https://orcid.org/0000-0003-3494-343X
Kat Barger https://orcid.org/0000-0001-5817-0932
Jorge Barrera-Ballesteros https://orcid.org/0000-0003-2405-7258
Julian Bautista https://orcid.org/0000-0002-9885-3989
Rachael L. Beaton https://orcid.org/0000-0002-1691-8217
Timothy C. Beers https://orcid.org/0000-0003-4573-6233
Matthew Bershady https://orcid.org/0000-0002-3131-4374
Dmitry Bizyaev https://orcid.org/0000-0002-3601-133X
Michael R. Blanton https://orcid.org/0000-0003-1641-6222
Jo Bovy https://orcid.org/0000-0001-6855-442X
William Nielsen Brandt https://orcid.org/0000-0002-0167-2453
Joel R. Brownstein https://orcid.org/0000-0002-8725-1069
Kevin Bundy https://orcid.org/0000-0001-9742-3138
Adam Burgasser https://orcid.org/0000-0002-6523-9536
Nell Byler https://orcid.org/0000-0002-7392-3637
Michele Cappellari https://orcid.org/0000-0002-1283-8420
Ricardo Carrera https://orcid.org/0000-0001-6143-8151
Yanping Chen https://orcid.org/0000-0001-8821-0309
Haeun Chung https://orcid.org/0000-0002-3043-2555
Kevin Covey https://orcid.org/0000-0001-6914-7797
Yu Sophia Dai https://orcid.org/0000-0002-7928-416
Jeremy Darling https://orcid.org/0000-0003-2511-2060
Kyle Dawson https://orcid.org/0000-0002-0553-3805
Nathan De Lee https://orcid.org/0000-0002-3657-0705
Niv Drory https://orcid.org/0000-0002-7339-3170
Eric Emsellem https://orcid.org/0000-0002-6155-7166
Diane Feuillet https://orcid.org/0000-0002-3101-5921
Scott W. Fleming https://orcid.org/0000-0003-0556-027X
Peter M. Frinchaboy https://orcid.org/0000-0002-0740-8346
Hai Fu https://orcid.org/0000-0001-9608-6395
Lluís Galbany https://orcid.org/0000-0002-1296-6887
Meng Gu https://orcid.org/0000-0002-4267-9344
Hong Guo https://orcid.org/0000-0003-4936-8247
Christian R. Hayes https://orcid.org/0000-0003-2969-2445
David W. Hogg https://orcid.org/0000-0003-2866-9403
Kelly Holley-Bockelmann https://orcid.org/0000-0003-2227-1322
Jon A. Holtzman https://orcid.org/0000-0002-9771-9622
Bau-Ching Hsieh https://orcid.org/0000-0001-5615-4904
Jason A. S. Hunt https://orcid.org/0000-0001-8917-1532
Ho Seong Hwang https://orcid.org/0000-0003-3428-7612
Héctor J. Ibarra-Medel https://orcid.org/0000-0002-9790-6313
Jennifer Johnson https://orcid.org/0000-0001-7258-1834
Henrik Jönsson https://orcid.org/0000-0002-4912-8609
Karen Kinemuchi https://orcid.org/0000-0001-7908-7724
Juna Kollmeier https://orcid.org/0000-0001-9852-1610
Kathryn Kreckel https://orcid.org/0000-0001-6551-3091
Sandor Kruk https://orcid.org/0000-0001-8010-8879
Ivan Lacerna https://orcid.org/0000-0002-7802-7356
Ting-Wen Lan https://orcid.org/0000-0001-8857-7020
David R. Law https://orcid.org/0000-0002-9402-186X
Jianhui Lian https://orcid.org/0000-0001-5258-1466
Lihwai Lin (林俐暉) https://orcid.org/0000-0001-7218-7407
Yen-Ting Lin https://orcid.org/0000-0001-7146-4687
Chris Lintott https://orcid.org/0000-0001-5578-359X
Steven R. Majewski https://orcid.org/0000-0003-2025-3147
Arturo Manchado https://orcid.org/0000-0002-3011-686X
Rui Marques-Chaves https://orcid.org/0000-0001-8442-1846
Karen L. Masters (何凱論) https://orcid.org/0000-0003-0846-9578
Michael Merrifield https://orcid.org/0000-0002-4202-4727
Dante Minniti https://orcid.org/0000-0002-7064-099X
Demitri Muna https://orcid.org/0000-0002-1631-4114
Jeffrey A. Newman https://orcid.org/0000-0001-8684-2222
Zach Pace https://orcid.org/0000-0003-4843-4185
Nelson Padilla https://orcid.org/0000-0001-9850-9419
Kaike Pan https://orcid.org/0000-0002-2835-2556
Hsi-An Pan https://orcid.org/0000-0002-1370-6964
Ismael Perez-Fournon https://orcid.org/0000-0002-2807-6459
Marc H. Pinsonneault https://orcid.org/0000-0002-7549-7766
Abhishek Prakash https://orcid.org/0000-0003-4451-4444
Hans-Walter Rix https://orcid.org/0000-0003-4996-9069
Annie C. Robin https://orcid.org/0000-0001-8654-9499
Alexandre Roman-Lopes https://orcid.org/0000-0002-1379-4204
Benjamin Rose https://orcid.org/0000-0002-1873-8973
Ashley J. Ross https://orcid.org/0000-0002-7522-9083
Kate H. R. Rubin https://orcid.org/0000-0001-6248-1864
Jaderson S. Schimoia https://orcid.org/0000-0002-5640-6697
Edward Schlafly https://orcid.org/0000-0002-3569-7421
David Schlegel https://orcid.org/0000-0002-5042-5088
Mathias Schultheis https://orcid.org/0000-0002-6590-1657
Shiyin Shen https://orcid.org/0000-0002-3073-5871
Jennifer Sobeck https://orcid.org/0000-0002-4989-0353
David V. Stark https://orcid.org/0000-0002-3746-2853
Keivan G. Stassun https://orcid.org/0000-0002-3481-9052
Matthias Steinmetz https://orcid.org/0000-0001-6516-7459
Thaisa Storchi-Bergmann https://orcid.org/0000-0003-1772-0023
Guy S. Stringfellow https://orcid.org/0000-0003-1479-3059
Jamie Tayar https://orcid.org/0000-0002-4818-7885
Patricia Tissera https://orcid.org/0000-0001-5242-2844
Nicholas W. Troup https://orcid.org/0000-0003-3248-3097
David Wake https://orcid.org/0000-0002-6047-1010
Kyle B. Westfall https://orcid.org/0000-0003-1809-6920
Renbin Yan https://orcid.org/0000-0003-1025-1711
Gail Zasowski https://orcid.org/0000-0001-6761-9359
Kai Zhang https://orcid.org/0000-0002-9808-3646
Zheng Zheng https://orcid.org/0000-0003-1887-6732
Guangtun Zhu https://orcid.org/0000-0002-7574-8078
Joel C. Zinn https://orcid.org/0000-0002-7550-7151
Hu Zou https://orcid.org/0000-0002-6684-3997

References

Abazajian, K. N., Adelman-McCarthy, J. K., Agüeros, M. A., et al. 2009, ApJS, 182, 543
Abolfathi, B., Aguado, D. S., Aguilar, G., et al. 2018, ApJS, 235, 42
Ahn, C. P., Alexandroff, R., Allende Prieto, C., et al. 2012, ApJS, 203, 21
Aihara, H., Allende Prieto, C., An, D., et al. 2011, ApJS, 193, 29
Alam, S., Albareti, F. D., Allende Prieto, C., et al. 2015, ApJS, 219, 12
Albareti, F. D., Allende Prieto, C., Almeida, A., et al. 2017, ApJS, 233, 25

Argudo-Fernández, M., Verley, S., Bergond, G., et al. 2015, A&A, 578, A110
Ata, M., Baumgarten, F., Bautista, J., et al. 2018, MNRAS, 473, 4773
Bailer-Jones, C. A. L., Rybizki, J., Fouesneau, M., Mantelet, G., & Andrae, R. 2018, AJ, 156, 58
Bautista, J. E., Vargas-Magaña, M., Dawson, K. S., et al. 2018, ApJ, 863, 110
Beifiori, A., Maraston, C., Thomas, D., & Johansson, J. 2011, A&A, 531, A109
Belfiore, F., Westfall, K. B., Schaefer, A., et al. 2019, AJ, submitted (arXiv:1901.00866)
Bernardi, M., Fischer, J.-L., Sheth, R. K., et al. 2017, MNRAS, 468, 2569
Blanton, M. R., Kazin, E., Muna, D., Weaver, B. A., & Price-Whelan, A. 2011, AJ, 142, 31
Blanton, M. R., Bershady, M. A., Abolfathi, B., et al. 2017, AJ, 154, 28
Bohlin, R. C., Mészáros, S., Fleming, S. W., et al. 2017, AJ, 153, 234
Boller, T., Freyberg, M. J., Trümper, J., et al. 2016, A&A, 588, A103
Bolton, A. S., Schlegel, D. J., Aubourg, É., et al. 2012, AJ, 144, 144
Bowen, I. S., & Vaughan, A. H., Jr 1973, ApOpt, 12, 1430
Bruzual, G., & Charlot, S. 2003, MNRAS, 344, 1000
Bruzual, A. G. 1983, ApJ, 273, 105
Bundy, K., Bershady, M. A., Law, D. R., et al. 2015, ApJ, 798, 7
Cappellari, M. 2017, MNRAS, 466, 798
Cappellari, M., & Copin, Y. 2003, MNRAS, 342, 345
Cappellari, M., & Emsellem, E. 2004, PASP, 116, 138
Chambers, K. C., Magnier, E. A., Metcalfe, N., et al. 2016, arXiv:1612.05560
Cherinka, B., Andrews, B. H., Sánchez-Gallego, J., et al. 2019, AJ, submitted (arXiv:1812.03833)
Cherinka, B., Sánchez-Gallego, J., Andrews, B., & Brownstein, J. 2018, sdss/marvin: Marvin Beta 2.2.5, Zenodo doi:10.5281/zenodo.1230529
Coffey, D., Salvato, M., Merloni, A., et al. 2018, A&A, submitted
Conroy, C. 2013, ARA&A, 51, 393
Conroy, C., & Gunn, J. E. 2010, FSPS: Flexible Stellar Population Synthesis, Astrophysics Source Code Library, ascl:1010.043
Dalcanton, J. J., Williams, B. F., Lang, D., et al. 2012, ApJS, 200, 18
Dawson, K. S., Kneib, J.-P., Percival, W. J., et al. 2016, AJ, 151, 44
DESI Collaboration, Aghamousa, A., Aguilar, J., et al. 2016, arXiv:1611.00036
Domínguez Sánchez, H., Huertas-Company, M., Bernardi, M., Tuccillo, D., & Fischer, J. L. 2018, MNRAS, 476, 3661
Donor, J., Frinchaboy, P. M., Cunha, K., et al. 2018, AJ, 156, 142
Drory, N., MacDonald, N., Bershady, M. A., et al. 2015, AJ, 149, 77
Dwelly, T., Salvato, M., Merloni, A., et al. 2017, MNRAS, 469, 1065
Eisenstein, D. J., Weinberg, D. H., Agol, E., et al. 2011, AJ, 142, 72
Etherington, J., & Thomas, D. 2015, MNRAS, 451, 660
Evans, D. W., Riello, M., De Angeli, F., et al. 2018, A&A, 616, A4
Falcón-Barroso, J., Sánchez-Blázquez, P., Vazdekis, A., et al. 2011, A&A, 532, A95
Finkbeiner, D. P., Schlafly, E. F., Schlegel, D. J., et al. 2016, ApJ, 822, 66
Fischer, J.-L., Bernardi, M., & Meert, A. 2017, MNRAS, 467, 490
Fischer, J.-L., Domínguez Sánchez, H., & Bernardi, M. 2018, MNRAS, submitted, (arXiv:1811.02580)
Frieman, J. A., Bassett, B., Becker, A., et al. 2008, AJ, 135, 338
Gaia Collaboration, Brown, A. G. A., Vallenari, A., et al. 2016, A&A, 595, A2
Gaia Collaboration, Brown, A. G. A., Vallenari, A., et al. 2018, A&A, 616, A1
Goddard, D., Thomas, D., Maraston, C., et al. 2017a, MNRAS, 466, 4731
Goddard, D., Thomas, D., Maraston, C., et al. 2017b, MNRAS, 465, 688
Grier, C. J., Trump, J. R., Shen, Y., et al. 2017, ApJ, 851, 21
Gunn, J. E., Siegmund, W. A., Mannery, E. J., et al. 2006, AJ, 131, 2332
Gupta, R. R., D'Andrea, C. B., Sako, M., et al. 2011, ApJ, 740, 92
Gustafsson, B., Edvardsson, B., Eriksson, K., et al. 2008, A&A, 486, 951
Hart, R. E., Bamford, S. P., Willett, K. W., et al. 2016, MNRAS, 461, 3663
Hayden, B. T., Gupta, R. R., Garnavich, P. M., et al. 2013, ApJ, 764, 191
Haynes, M. P., Giovanelli, R., Kent, B. R., et al. 2018, ApJ, 861, 49
Hemler, Z., Grier, C., Brandt, W., et al. 2018, ApJ, in press (arXiv:1811.00010)
Høg, E., Fabricius, C., Makarov, V. V., et al. 2000, A&A, 355, L27
Holtzman, J. A., Shetrone, M., Johnson, J. A., et al. 2015, AJ, 150, 148
Holtzman, J. A., Hasselquist, S., Shetrone, M., et al. 2018, AJ, 156, 125
Hunter, J. D. 2007, CSE, 9, 90
Hutchinson, T. A., Bolton, A. S., Dawson, K. S., et al. 2016, AJ, 152, 205
Jensen, T. W., Vivek, M., Dawson, K. S., et al. 2016, ApJ, 833, 199
Jones, E., Oliphant, T., Peterson, P., et al. 2001, SciPy: Open Source Scientific Tools for Python, http://www.scipy.org
Jönsson, H., Allende Prieto, C., Holtzman, J. A., et al. 2018, AJ, 156, 126
Koleva, M., Prugniel, P., Bouchard, A., & Wu, Y. 2009, A&A, 501, 1269
Koleva, M., Prugniel, P., Bouchard, A., & Wu, Y. 2011, ULySS: A Full Spectrum Fitting Package, Astrophysics Source Code Library, ascl:1104.007
Kollmeier, J. A., Zasowski, G., Rix, H.-W., et al. 2017, arXiv:1711.03234
Kurucz, R. L. 1979, ApJS, 40, 1
Kurucz, R. L., & Avrett, E. H. 1981, SAOSR, 391
Lampeitl, H., Smith, M., Nichol, R. C., et al. 2010, ApJ, 722, 566
Law, D. R., Yan, R., Bershady, M. A., et al. 2015, AJ, 150, 19
Law, D. R., Cherinka, B., Yan, R., et al. 2016, AJ, 152, 83
Leitherer, C., Schaerer, D., Goldader, J. D., et al. 1999, ApJS, 123, 3
Li, N., & Thakar, A. R. 2008, CSE, 10, 18
Luo, A.-L., Zhao, Y.-H., Zhao, G., et al. 2015, RAA, 15, 1095
MacLeod, C. L., Green, P. J., Anderson, S. F., et al. 2018, AJ, 155, 6
Majewski, S. R., Schiavon, R. P., Frinchaboy, P. M., et al. 2017, AJ, 154, 94
Maraston, C. 2005, MNRAS, 362, 799
Maraston, C., & Strömbäck, G. 2011, MNRAS, 418, 2785
Masters, K., Stark, D., Pace, Z., et al. 2018, MNRAS, submitted (arXiv:1901.05579)
Meert, A., Vikram, V., & Bernardi, M. 2013, MNRAS, 433, 1344
Meert, A., Vikram, V., & Bernardi, M. 2015, MNRAS, 446, 3943
Meert, A., Vikram, V., & Bernardi, M. 2016, MNRAS, 455, 2440
Morganson, E., Green, P. J., Anderson, S. F., et al. 2015, ApJ, 806, 244
Myers, A. D., Palanque-Delabrouille, N., Prakash, A., et al. 2015, ApJS, 221, 27
Nair, P. B., & Abraham, R. G. 2010, ApJS, 186, 427
Ness, M., Hogg, D. W., Rix, H.-W., Ho, A. Y. Q., & Zasowski, G. 2015, ApJ, 808, 16
Oke, J. B., & Shipman, H. L. 1971, in IAU Symp. 42, White Dwarfs, ed. W. J. Luyten (Dordrecht: Springer), 67
Palanque-Delabrouille, N., Magneville, C., Yèche, C., et al. 2016, A&A, 587, A41
Parikh, T., Thomas, D., Maraston, C., et al. 2018, MNRAS, 477, 3954
Penny, S. J., Masters, K. L., Weijmans, A.-M., et al. 2016, MNRAS, 462, 3955
Pérez, F., & Granger, B. E. 2007, CSE, 9, 21
Pinsonneault, M. H., Elsworth, Y. P., Tayar, J., et al. 2018, ApJS, 239, 32
Prakash, A., Licquia, T. C., Newman, J. A., et al. 2016, ApJS, 224, 34
Predehl, P., Andritschke, R., Becker, W., et al. 2014, Proc. SPIE, 9144, 91441T
Raddick, M. J., Thakar, A. R., Szalay, A. S., & Santos, R. D. C. 2014a, CSE, 16, 22
Raddick, M. J., Thakar, A. R., Szalay, A. S., & Santos, R. D. C. 2014b, CSE, 16, 32
Raichoor, A., Comparat, J., Delubac, T., et al. 2017, MNRAS, 471, 3955
Reid, B., Ho, S., Padmanabhan, N., et al. 2016, MNRAS, 455, 1553
Reynolds, A. P., de Bruijne, J. H. J., Perryman, M. A. C., Peacock, A., & Bridge, C. M. 2003, A&A, 400, 1209
Rigault, M., Copin, Y., Aldering, G., et al. 2013, A&A, 560, A66
Robitaille, T. P., Tollerud, E. J., Greenfield, P., et al. 2013, A&A, 588, A33
Ruan, J. J., Anderson, S. F., Green, P. J., et al. 2016, ApJ, 825, 137
Salvato, M., Buchner, J., Budavári, T., et al. 2018, MNRAS, 473, 4937
Sánchez, S. F., Pérez, E., Sánchez-Blázquez, P., et al. 2016, RMxAA, 52, 171
Sánchez, S. F., Avila-Reese, V., Hernandez-Toledo, H., et al. 2018, RMxAA, 54, 217
Sánchez-Blázquez, P., Peletier, R. F., Jiménez-Vicente, J., et al. 2006, MNRAS, 371, 703
Saxton, R. D., Read, A. M., Esquej, P., et al. 2008, A&A, 480, 611
Schlegel, D. J., Finkbeiner, D. P., & Davis, M. 1998, ApJ, 500, 525
Smee, S. A., Gunn, J. E., Uomoto, A., et al. 2013, AJ, 146, 32
Stoughton, C., Lupton, R. H., Bernardi, M., et al. 2002, AJ, 123, 485
Talbot, M. S., Brownstein, J. R., Bolton, A. S., et al. 2018, MNRAS, 477, 195
Taylor, M. B. 2005, in Proc. ASP Conf. Ser. 347, adass XIV, ed. P. Shopbell, M. Britton, & R. Ebert (San Francisco, CA: ASP), 29
Thakar, A. R. 2008, CSE, 10, 9
Thakar, A. R., Szalay, A., Fekete, G., & Gray, J. 2008, CSE, 10, 30
Trager, S. C., Worthey, G., Faber, S. M., Burstein, D., & González, J. J. 1998, ApJS, 116, 1
van der Walt, S., Colbert, S. C., & Varoquaux, G. 2011, CSE, 13, 22
Vazdekis, A., Sánchez-Blázquez, P., Falcón-Barroso, J., et al. 2010, MNRAS, 404, 1639
Wake, D. A., Bundy, K., Diamond-Stanic, A. M., et al. 2017, AJ, 154, 86
Wang, H., Mo, H. J., Jing, Y. P., et al. 2009, MNRAS, 394, 398
Wang, H., Mo, H. J., Yang, X., & van den Bosch, F. C. 2012, MNRAS, 420, 1809
Weil, S. A., Brandt, S. A., Miller, E. L., Long, D. D. E., & Maltzahn, C. 2006, in Proc. 7th Symp. Operating Systems Design and Implementation, OSDI '06 (Berkeley, CA: USENIX Association), 307
Westfall, K. B., Cappellari, M., Bershady, M. A., et al. 2019, AJ, submitted (arXiv:1901.00856)
Wilkinson, D. M., Maraston, C., Goddard, D., Thomas, D., & Parikh, T. 2017, MNRAS, 472, 4297

Willett, K. W., Lintott, C. J., Bamford, S. P., et al. 2013, MNRAS, 435, 2835
Wilson, J., Hearty, F., Skrutskie, M., et al. 2018, PASP, in press
Worthey, G., & Ottaviani, D. L. 1997, ApJS, 111, 377
Yan, R., Chen, Y., Lazarz, D., et al. 2018, ApJ, submitted
Yan, R., Bundy, K., Law, D. R., et al. 2016a, AJ, 152, 197
Yan, R., Tremonti, C., Bershady, M. A., et al. 2016b, AJ, 151, 8
Yang, X., Mo, H. J., van den Bosch, F. C., et al. 2007, ApJ, 671, 153
Yanny, B., Rockosi, C., Newberg, H. J., et al. 2009, AJ, 137, 4377
York, D. G., Adelman, J., Anderson, J. E., Jr., et al. 2000, AJ, 120, 1579
Zasowski, G., Cohen, R. E., Chojnowski, S. D., et al. 2017, AJ, 154, 198
Zheng, Z., Wang, H., Ge, J., et al. 2017, MNRAS, 465, 4572